약학박사학위논문

Identification of Tentonin 3, a Novel Mechanosensitive Channel and Its Role in Proprioception

새로운 기계수용채널 Tentonin 3의 클로닝 및 자가 수용 감각 역할 연구

2016년 8월

서울대학교 대학원

분자의학 및 바이오제약학과

분자의학 및 바이오제약학 전공

홍 규 상

Abstract

Touch sensation or proprioception requires the transduction of mechanical stimuli into electrical signals by mechanoreceptors in the periphery. These mechanoreceptors are equipped with various transducer channels. Although Piezo1 and 2 are mechanically activated (MA) channels with rapid inactivation, MA molecules with other inactivation kinetics have not been identified. Here we report that heterologously expressed Tentonin3 (TTN3)/TMEM150C is activated by mechanical stimuli with distinctly slow inactivation kinetics. Genetic ablation of *Ttn3*/*Tmem150c* markedly reduced slowly adapting neurons in dorsal-root ganglion neurons. The mechanically-activated TTN3 currents were inhibited by known-blockers of mechanosensitive ion channels. Moreover, TTN3 was localized in muscle spindle afferents. *Ttn3*-deficient mice exhibited the loss of coordinated movements and abnormal gait. Thus, TTN3 appears to be a component of a mechanosensitive channel with a slow inactivation rate and contributes to motor coordination. Identification of this gene advances our understanding of the various types of mechanosensations including proprioception.

Keywords: Mechanosensation; Proprioception; Mechanosensitive ion channel; TMEM150C; Tentonin 3.

Student number: 2010-24243

Table of Contents

List of Figures

List of Table

INTRODUCTION

1. Mechanosensation

Mechanosensation is the sensation of external and internal mechanical stimuli and is essential for living organisms. It has been evolved from eubacteria for cell protection and survival. In mammals, it is required for tactile sensation, proprioception, and nociception(Delmas and Coste, 2013) . In addition, physiological functions such as hearing, body balance, baroreceptor reflex, myogenic activity of blood vessels, and blood volume control in the kidneys require the sensing of mechanical stimuli (Arnadottir and Chalfie, 2010; Sukharev and Sachs, 2012). All physiological mechanosensations are the conversion of mechanical stimuli into neuronal signals.

In mammals, DRG sensory neurons extend their axons to the periphery, forming various types of mechanoreceptors in our body. These nerve endings of mechanoreceptors are localized all over the skin. This is called somatosensory system which detects touch and pain. Sound wave is sensed by inner and outer hair cells in ears. Baroreflex system regulates blood pressure near heart and muscle spindle is activated by skeletal muscle stretch to coordinate our body position and movement. These mechanoreceptors equipped with MS ion channels that is activated by stretch

or deformation of cell plasma membrane. Therefore, when touch stimuli activate MS ion channels in specific mechanoreceptors or connected nerve endings, action potential fires and this signal directly goes to our brain through sensory neurons.

1.1. Somatosensory system

Somatosensory system is essential for the activities of daily life, such as recognizing or grabbing` objects, walking, communicating with others, eating food, and even maternal nursing. Tactile stimuli are detected by specialized end organs in the skin such as Meissner corpuscles, Merkel cell neurite complex, Ruffini endings, Pacinian corpuscles, and other end organs in hair follicles. When these organs are stimulated, neural signal is generated and transmitted to the spinal cord through the primary afferent nerves(Zimmerman et al., 2014). These cutaneous mechanoreceptors are divided into low and high threshold mechanoreceptors, or rapidly and slowly adapting receptors, depending on their response to sustained mechanical stimuli (Delmas et al., 2011)(Fig. 1).

In the skin, light brush or gentle wind is sensed by hair follicles –G-hair and D-hair, innervated by A-beta and A-delta nerves. Meissner corpuscle senses dynamic

deformation of the skin or sensitive touch with rapid adapting response in small receptive fields, innervating to A-beta nerve which is localized in shallow dermis. Merkel cell neurite complex is also localized in shallow dermis and relatively well understood. This peripheral neuron complex is connected to A-beta nerve and is excited by light touch and indentation depth with slow adapting response. Ruffini ending is activated by stretch or gentle pressure with slow adapting response and localized in middle of dermis connecting with A-beta nerve. Pacinian corpuscle forms relatively big complex with a capsule-like structure in deep dermis, innervated by A beta nerve and senses vibration or pressure with rapid adapting manner. Furthermore, C-fiber nerve endings are located in epidermal region to mediate touch with slow adapting firing. These receptors are classified as low threshold mechanoreceptors. High threshold mechanoreceptor is mechano-nociceptors which mediates injurious force with very slow adapting response. This receptor is innervated with C- and A-delta fibers and located in epidermal region of the shallow skin (Delmas et al., 2011). The morphology, location in the skin, and the sensitivity or adaptation property of the mechanoreceptors provide a rich repertoire of tactile discrimination.

Receptor subtype	Hair follicles	Meissner corpuscle	Pacinian corpuscle	Merkel cell–neurite complex	Ruffini corpuscle	C-fibre LTM	Mechano-nociceptor Polymodal nociceptor
Skin stimulus	Light brush	Dynamic deformation	Vibration	Indentation depth	Stretch	Touch	Injurious forces
	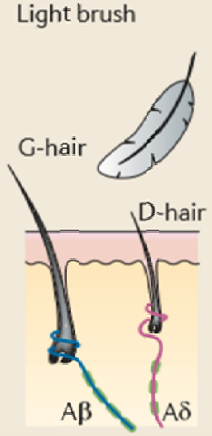	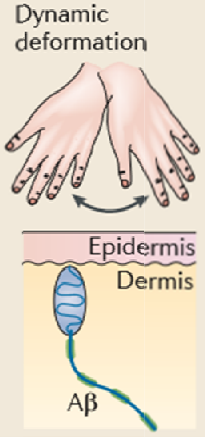	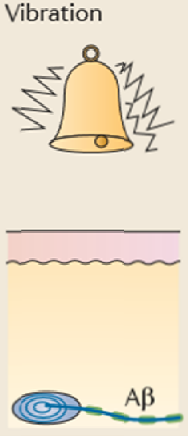	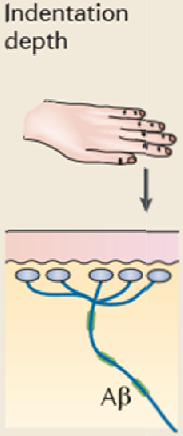	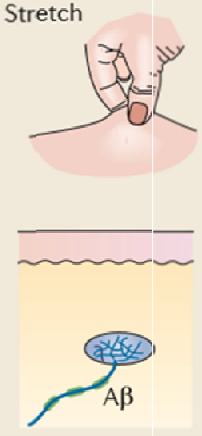	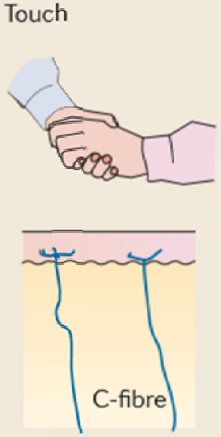	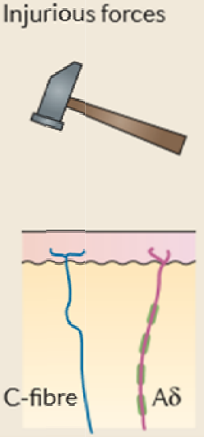
Afferent response	RA, LT	RA, LT	RA, LT	SA, LT	SA, LT	SA, LT	SA, HT
							
Stimulus							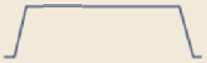
Receptive field	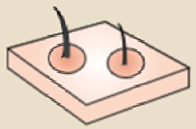	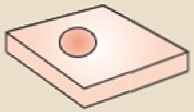	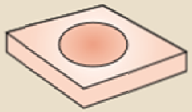	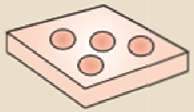	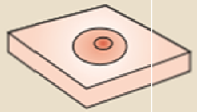		
Perceptual functions	Skin movement	Skin motion; detecting slipping objects	Vibratory cues transmitted by body contact when grasping an object	Fine tactile discrimination; form and texture perception	Skin stretch; direction of object motion, hand shape and finger position	Pleasant contact; social interaction	Skin injury; pain

Figure 1. Cutaneous somatosensory receptors in mammals (Delmas et al., 2011).

There are various types of mechanoreceptors in the skin. Sensory neurons extend their axons to form synapse to peripheral neurons or nerve endings by themselves and detect somatosensory information. RA (rapidly adapting), SA (slowly adapting), LT (low threshold) and HT (high threshold)

1.2. Auditory system

Hair cells in the sensory epithelium of the cochlea known as the organ of Corti are the key component of auditory mechanotransduction in animal. When sound wave touches outer hair cells (OHC) and inner hair cells (IHC), MS ion channels are activated, sound is converted into electrical action potential and this signal is transmitted to central nervous system. Therefore, we can hear every sound via MS ion channels that expressed in hair cells.

MS ion channel complex is expressed in the hair bundle of each hair cell which is comprised of three graded stereocilia. The tip-link which is composed of mainly two adaptor proteins such as protocadherin-15 and cadherin-23 is connecting two stereocilia (Ahmed et al., 2006; Siemens et al., 2004) (Fig. 2). This link is connected to MS ion channel in hair cell plasma membrane and plays key component machinery in auditory mechanotransduction.

TMC1 is a strong candidate for MS ion channel in auditory system. Mutations of TMC1 cause dominant and recessive non syndromic hearing losses and 29 pathogenic mutations have been identified to result in deafness in human (Holt et al., 2014; Kurima et al., 2002). IHC and OHC express TMC1 and TMC2, another member of TMC family and KO of both genes causes complete loss of hair cell

mechanotransduction (Kawashima et al., 2011). Furthermore, Ca^{2+} permeability and single channel conductance elicited by mechanical stimulation were significantly changed in TMC1 and TMC2 mutation mouse (Pan et al., 2013).

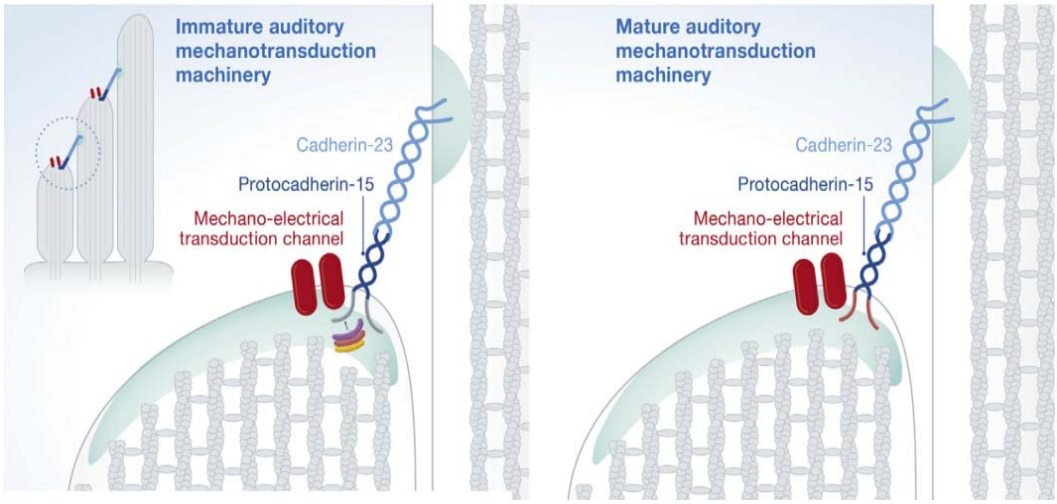

Figure 2. A schematic diagram of auditory mechanotrasnduction machinery in hair cell (Pepermans and Petit, 2015).

Composition of tip-link and MS channel complex in Immature (left) and mature auditory hair cells (right).

From these studies, it is obvious that TMC1 is one of essential component of MS ion channel complex in hair cell mechanotransduction. However, it is still controversial that TMC1 forms the core of MS ion channel because many previous reports evidenced only modulatory effects of TMC1 not direct mechanisms as a MS ion channel.

1.3. Baroreceptor reflex

Baroreceptor reflex is a crucial repairing system for blood pressure and oxygenation for survival of all animals. Baroreceptor is one type of mechanoreceptor sensory neuron localized in blood vessels and MS ion channels thought to be expressed in this receptor. MS ion channel is activated by stretch of blood vessel, baroreceptor fires action potential and this signal is conveyed to the petrosal, nodose and DRG sensory neurons to medulla to regulate the proper blood pressure (Abboud and Benson, 2015).

Recent study provided that Acid-Sensing Ion Channel 2b (ASIC2), which is interestingly not activated by pH change itself, is highly expressed in nodose neurons and baroreceptor endings. Moreover, ASIC2 KO mouse showed significantly

decreased mechanosensitive currents in baroreceptor neurons, abnormal sympathetic control and decreased gain of the baroreflex (Lu et al., 2009). Thus, this study indicates ASIC2 maybe participate in MS ion channel complex in baroreceptors. However, no study has been proven direct mechanosensitivity of ASIC2 expressed in cell line.

1.4. Proprioception

Proprioception is a sense of limb position and movement. Proprioceptive sensory signals are essential for coordinated movements including locomotion (Proske and Gandevia, 2012). Proprioception involves sensory inputs from muscles, skin, joints and tendons. Among these sensory inputs, muscle spindle (MS) afferents play a key role in proprioception (Rossi-Durand, 2006).

MS is composed of encapsulated intrafusal muscles that are innervated with group Ia and II sensory afferents (Proske and Gandevia, 2012; Rossi-Durand, 2006)(Fig. 3). MS afferents project to the ventral horn of the spinal cord where they are mono-synaptically connected to motor neurons or interneurons to transmit signals to brain. They are sensitive to passive muscle stretch or contraction. Thus, the neural

responses to muscle stretch of MS afferents are key signals to coordinate body movements (Proske and Gandevia, 2012). Deafferentation or genetic disruption of MS induces neurological deficits such as gait ataxia with loss of central pattern generation of locomotion (Tourtellotte and Milbrandt, 1998). In addition, changes in proprioception such as fatigue after exhaustive exercise, aging, or Parkinson disease often lead to injury due to loss of motor coordination (Proske and Gandevia, 2012).

MS ion channel must be localized in innervated afferents of muscle spindle. When the muscle is stretched, MS ion channel is activated, action potential is generated and this signal is transmitted to the central nervous system. Thus MS ion channel is crucial for understanding muscle movement, however, molecular identity has not been found yet. Recently, Piezo2 was found to be involved in proprioception in mouse. Piezo2 is present in muscle spindles and its genetic deletion from muscle afferents leads to marked reduction in stretch-induced nerve activity of muscle spindle afferents as well as prominent loss of muscle coordination (Woo et al., 2015a). This does not preclude the possible presence of other MA channels. The inactivation kinetic of Piezo2 does not fit to the kinetics of MS afferent responses. Piezo2 inactivates rapidly with a brief activation period whereas most MS afferents burst its action potentials as long as muscle stretches last.

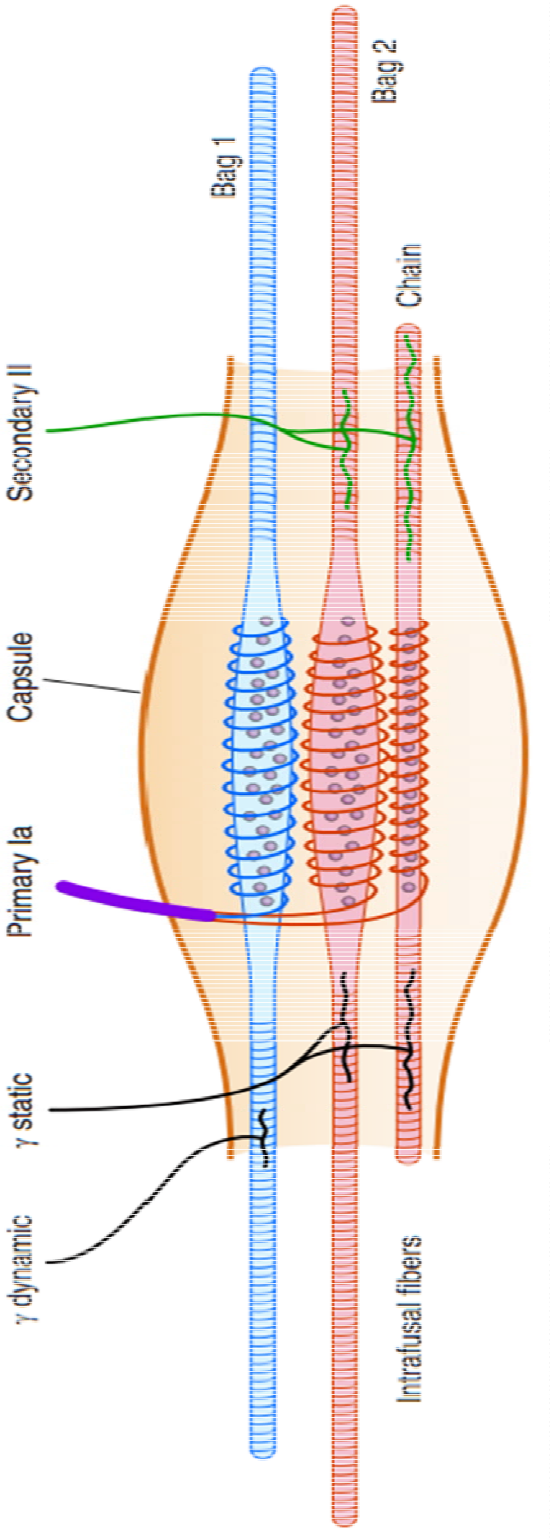
Bag 1
Bag 2
Chain
Secondary II
Capsule
Primary Ia
γ static
γ dynamic
Intrafusal fibers

Figure 3. Structure of muscle spindle and its primary endings (Proske and Gandevia, 2012).

Muscle spindle is comprised of large nuclear bag1 and 2 fibers and several small chain fibers that is collectively called intrafusal muscle fibers. These fibers are innervated by sensory nerve endings, forming annular spiral structure. MS ion channels are thought to be present in this nerve endings and activated by muscle stretch to regulate motor coordination.

2. Ion Channels

2.1. Overview

Ion channels are pore-forming proteins that comprise of more than two transmembrane domains (TMs) and bind on the lipid bilayers such as a plasma membrane or other intracellular microorganelles -mitochondria, lysosome and autophagosome. The critical function of ion channel in the cell is ion conducting property which leads to membrane potential change which in turn regulates physiology of our body. A variety of intrinsic or extrinsic factors –hormones, chemicals, peptides, membrane potential change, mechanical force as well as heat and cold temperature are detected by each different types of ion channels, which are followed by conformational change and resulted in opening its pore. Thus, electrical signal is generated by ion conduction through the channel pore. This electrical signal performs powerful communicating role to maintain not only each cells but our whole body (Ashcroft, 2000). This transition of membrane potential alters intracellular ion composition of each cell and affects a variety of signaling pathways such as Ca^{2+}-mediated transcriptional change. And also most of this electrical signals turn into action potential (AP) to transmit to the central nervous system (CNS) and regulates sensory transduction including visual, olfactory, auditory, gustatory and

somatosensory system. Defects of ion channels incur profound physiological effects such as cruel diseases so their functional study is essential to understand our body.

2.2. Classification of ion channels

On the criteria by conducting type of ions, ion channels can be classified as cation and anion channels. Anion channels mainly conduct chloride (Cl^-) and are categorized into four groups by their function: voltage-gated chloride channels (ClCs), cystic fibrosis transmembrane conductance regulator (CFTR), ligand-gated chloride channels, volume-regulated chloride channels and calcium-activated chloride channels (CaCCs). Cation channels are categorized into five groups: proton (H^+) channels, sodium (Na^+) channels, potassium (K^+) channels, calcium (Ca^{2+}) channels and non-selective cation channels.

Ion channels can also be classified by gating mechanisms. Voltage-gated Na^+ and K^+ channels are responsible for action potential and voltage-gated Ca^{2+} channels have a crucial role in muscle contraction and transmitter release. Transient receptor potential (TRP) channels are activated by chemicals, $[Ca^{2+}]_i$, osmolarity and temperature. Cyclic nucleotide-gated channels are activated by cAMP and cGMP.

There are many types of ligand-gated ion channels such as acetylcholine, glutamate, ATP and gamma-aminobutyric acid (GABA) A receptors. Furthermore, channelodopsins are light-gated channels and mechanosensitive ion channels are activated by hearing, touch and pressure (Ashcroft, 2000).

3. Mechanosensitive ion channels

Mechanosensitive (MS) channels are ion channels that are activated by deformation of lipid bilayer membrane existed in all type cells (Delmas and Coste, 2013). It was firstly observed by Falguni Guharay and Frederick Sachs in chick skeletal muscles (Guharay and Sachs, 1984). MS channels represent various types of ion channels with different biophysical properties. This type of channels opens its pore by deformation of plasma membrane. Because of technical difficulties and functional redundancy to characterize MS channels, no many discoveries have been achieved. Although the large- and small-conductance mechanosensitive channels (MsC) responsible for osmotic shock in prokaryote are well characterized, there are no homologs in an animal (Kung, 2005).

In mammalian sensory system, MS channels can be characterized by sensitivity: low threshold (LT) and high threshold (HT), identified from thousands of single patch clamp in isolated DRG neurons (Cho et al., 2002). And also there are mainly three types of MS currents in isolated DRG neurons, determined by inactivation time kinetics under whole-cell patch mode: rapidly adapting (RA) currents (~10 ms), intermediately adapting (IA) currents (10 ms–30 ms) and slowly adapting (SA) currents (>30 ms) (Hu and Lewin, 2006) (Fig. 4). These MS currents reveal in DRG neurons and they were thought to be present in nerve endings of DRG axons to mediate all mechanotransduction in sensory system. Thus, it has been a long sought to identify the novel MS ion channels, and various candidates have been reported for modulatory effects of MS ion channels. However, no noticeable observations were made. In 2010, Patapoutian group reported a surprising discovery using DNA chips. They found Piezo1 and 2 are MS ion channels with distinctly fast inactivation kinetics when expressed cell line. This was the first MS ion channels in mammalian sensory system.

However, since Piezo2 KO mouse showed decreased RA MA current in DRG neurons, other molecular identity of IA or SA currents are unknown. To understand mammalian physiological functions, it is essential to discover MS ion channels other than Piezo2 in mammalian sensory system.

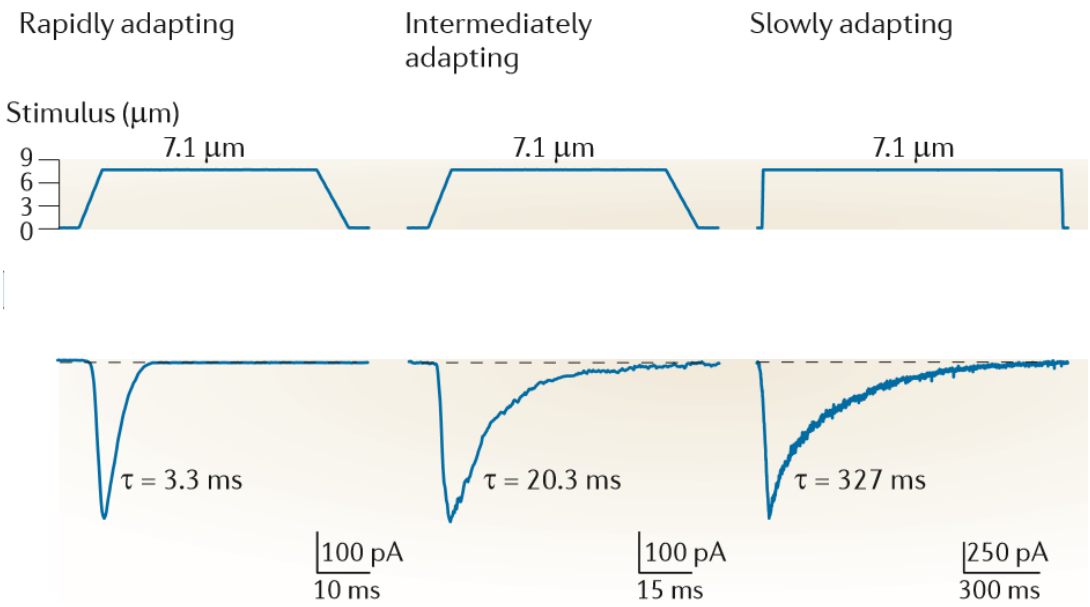

Figure 4. Three types of MS currents in DRG neurons (Delmas et al., 2011).

Representative traces of RA (rapidly adapting), IA (intermediately adapting) and SA (slowly adapting) mechanosensitive current in DRG sensory neurons. These current was characterized by distinct inactivation kinetics RA(<10 ms), IA (10-30 ms) and SA (>30). Generally, one DRG neuron reveals one type of MS current.

3.1. DEG/ENaC and TRPA1 in *Caenorhabditis elegans*

In *Caenorhabditis elegans*, ASH neuron which is a polymodal nociceptor detects defensive avoidance by multiple aversive stimuli, including chemicals, osmotic and mechanical cues such as harsh nose touch. In ASH neurons, MS current is highly sensitive to amiloride mediated by sodium ions and DEG/ENaC channels responsible for this phenomenon. Ablation of deg-1 and unc-8 genes (DEG/ENaC) reduce 80% of the MS currents in ASH neurons. Mutation in the pore region of DEG-1 changes ionic permeability, suggesting that DEG-1 channel is pore-forming subunit of the MS channel in ASH neurons (Geffeney et al., 2011). Multidendritic PVD neurons are another type of nociceptiors that detect noxious mechanical stimuli. When the DEG/ENaC genes are disrupted in this neuron, this *C. elegans* reveals no harsh touch escape behavior (Chatzigeorgiou et al., 2010). *C. elegans* TRPA1 (transient receptor potential ankyrin 1) was reported to form mechanosensitive ion channel of inner ear and *C. elegans* TRPA1 is activated by mechanical stimulation when overexpressed in mammalian cell line

3.2. MS channels in *Drosophila melanogaster*

Class III and IV dendritic arborization neurons exist in the body wall of *Drosophila* larvae and its function is to sense gentle touch sensation and noxious mechanical and heat stimuli, respectively. NOMPC is a member of the TRPN cation channel subfamily in *Drosophila melanogaster* and *C.elegans*. TRPN1 expresses highly in the soma and dendrites of class III neurons and genetic ablation of trpn1 fail to respond to touch stimuli (Yan et al., 2013). In class IV neurons, recently identified dmpiezo is responsible for mechanical nociception but not gentle touch or noxious heat sensation. Notably, electrophysiological study shows that heterologous expression of this gene generates rapidly adapting MS currents (Kim et al., 2012). This implies the presence of other types of MS ion channels in *Drosophila*.

3.3. Candidates for MS ion channels in mammal

3.3.1. TRPA1

Mammalian TRPA1 is highly expressed in small-diameter sensory neurons and this suggests its possible role in mechanical pain (Nagata et al., 2005). TRPA1 knock-out (KO) mouse revealed reduced acute noxious mechanical pain and seem to have

a role in mechanical hyperalgesia because mechanical pain threshold after bradykinin-mediated inflammation was significantly increased in TRPA1 KO mouse (Kwan et al., 2006). Furthermore, TRPA1 KO mouse showed decreased firing rates of C-fiber nociceptors by noxious mechanical stimuli in skin-nerve preparations (Brierley et al., 2009) and decreased population of slow-adapting mechanosensitive currents in DRG neurons (Vilceanu and Stucky, 2010). However, TRPA1 remains uncertain due to the lack of direct mechanical current in heterologous system.

3.3.2. Acid-sensing ion channels

Acid-sensing ion channels (ASICs) are pH sensitive proton-gated degenerin-epithelial Na^+ channel family. Because ASICs are homologues with MEC subunit and they are expressed in DRG neurons and peripheral mechanoreceptors as well as nociceptors. ASIC1A KO mouse showed significantly increased mechanical sensitivity of gut afferents while revealed no change of cutaneous touch sensation (Page et al., 2004). Ablation effect of ASIC2 is controversial because some groups reported that ASIC2 KO mouse showed decreased sensitivity of rapidly adapting cutaneous LTMs but the other group was found to be completely normal sensitivity of cutaneous touch in ASIC2 KO mouse (Price et al., 2001; Roza et al., 2004). Recently ASIC2 is highly

expressed in baroreceptor neurons and involved in baroreceptor sensitivity and controls blood pressure, thus ASIC2 KO mouse showed reduced mechanosensitivity resulted in hypertension (Lu et al., 2009). Ablation of ASIC3 exhibited decreased cutaneous noxious mechanical pain and mechanosensitivity of visceral afferents (Mogil et al., 2005).

Various implications in mechanosensation of ASICs have been reported, however, direct mechanical activation is lacking. Thus these data suggest ASICs contribute to indirect mechanism of mechanotransduction in mammal.

3.3.3. TREK1, TREK2 and TRAAK

K^+ channels are generally recognized as voltage sensor, but these channels are not activated by transition of membrane potential. They belong to two-pore domain K^+ channel (K2P) family. TREK1 is highly expressed in DRG nociceptors and activated by heat and pressure, determined by single patch clamp (Maingret et al., 2000). TREK1 KO mouse showed increased sensitivity to mechanical touch and heat but not to noxious mechanical pressure, thus in inflammation condition, this mouse significantly upregulated mechanical and thermal hyperalgesia (Alloui et al., 2006).

TREK2 and TRAAK are also expressed in DRG neurons and activated by plasma membrane stretch. TREK1 and TRAAK are thought to play together in mechanosensation. Because while TRAAK KO mice displayed significantly increased mechanosensitivity, silence of TREK1 further augmented this phenomenon (Noel et al., 2009).

Although many studies showed that K^+ channels are involved in mechanosensation, it is still unclear that these channels directly regulate mechanoperception in mammals or affect mechanosensitivity as modulators.

3.3.4. Piezo family

Piezo family was discovered by siRNA screening from DNA chip assay. Neuroblastoma cell line was known to reveal RA type MS current, thus siRNA candidates were introduced into this cell line to see the effect of RA current inhibition. Piezo1 and 2 were both activated by mechanical touch when overexpressed in cell line with fast inactivation kinetics (Coste et al., 2010). These channels form unique structure with enormous protein complex comprising more than 30 transmembrane

domains and involved not only in sensory transduction but also in various mechanosensations in mammals.

3.3.4.1. Tethering evidence of Piezos

Piezo1 and 2 are activated by direct mechanical touch without help of other molecules. When Piezo1 protein was purified and reconstituted in artificial lipid bilayers, it was activated by direct pressure and the property of the MA current was similar to the current in cell line. And also no interacting molecules were found, determined by protein association works (Coste et al., 2012). However, there are several associating modulators of Piezos. Piezo1 was co-immunoprecipitated with polycystin 2 (PC2) that is a member of TRP family and PC2 inhibited piezo1 activation sensitivity in renal epithelial tubular cells (Peyronnet et al., 2013). Furthermore, STOML3 (stomatin-like protein 3), which is a mammalian ortholue of C.elegans MEC-2 was found to be interact with Piezo1 and 2. Increased mechanical sensitivity and modulatory effect of Piezos were observed when co-expressed with STOML3 (Poole et al., 2014).

3.3.4.2. Sensory transduction of Piezo2

In sensory neurons, Piezo2 is expressed in relatively large DRG neurons and some part of nociceptors. Since Piezo2 mediated RA current in DRG was increased by bradykinin and Epac-1 agonist, it could be involved in mechanical hyperalgesia or allodynia (Dubin et al., 2012; Eijkelkamp et al., 2013). Two independent groups found that Piezo2 is expressed Merkel cell neurite complex and mediates slowly adapting cutaneous response in mouse. They found Mekel cell neurite complex synaptically connected to DRG nerve endings and possibly mechanoreception may occur in both site (Ikeda et al., 2014; Woo et al., 2014).

3.3.4.3. Function of Piezo1 in other tissues

Unlike Piezo2, Piezo1 is expressed in a variety of regions including lung, bladder, kidney, blood vessels, suggesting that it might have various function (Coste et al., 2010). Piezo1 is expressed in urothelial cells in the bladder. Mechanical stretch of this cell activates piezo1 and regulates ATP release, thus bladder stretch may be sensed by piezo1 (Peyronnet et al., 2013). Endothelial cells of developing blood vessels also express piezo1 in mouse. Ablation of Piezo1 in endothelial cells causes

defects in cellular alignment due to laminar shear stress (Ranade et al., 2014). In the kidney, Piezo1 was detected in isolated proximal tubules and activated by stretch induced mechanical stimuli in proximal convoluted tubule epithelial cells. This suggests that piezo1 might be involved in pressure of urine flow sensing (Miyamoto et al., 2014). According to a recent report, Piezo1 was detected in human neural stem cell (hNSC). hNSC was gradually activated by mechanical steps and this was abolished by *PIEZO1* knock-down. Myosin II-dependent traction forces generated local membrane tension and allowed PIEZO1-mediated transient Ca^{2+} influx, resulted in changes of hNSC differentiation (Pathak et al., 2014).

All these studies suggest that Piezo family is not only involved in sensory transduction but also participated in a variety of physiological functions of mechanosensation.

Purpose of This Study

Mechanotransduction is essential for all living organism to communicate with environment as well as to protect our body. Somatosensation, hearing, baroreceptor reflex and myogenic control of blood vessels are involved in this mechanism and these fundamental roles of an animal are mediated by mechanosensitive (MS) ion channels in molecular level. Therefore, identification and characterization of MS ion channels would be the first step to understand physiological function of mechanotransduction in our body.

There are mainly three types of mechanosensitive currents for mechanotransduction. Rapidly adapting (RA), intermediately adapting (IA) and slowly adapting (SA) MS currents were exhibited in DRG neurons. Thus, at least more than three different types of MS ion channels are possibly involved in mechanotransduction in mammals. However, the molecular identity of MS ion channels has not been known for several decades. Very recently, Piezo2 was discovered as RA MS ion channel in DRG neurons and this channel is expressed in Merkel cell neurite complex which mediates light touch in (Coste et al., 2010; Woo et al., 2014).

To identify a novel MS ion channel other than Piezo family, we screened channel like genes by means of DNA microarray analysis. From a number of candidates, one gene was cloned and characterized the properties and uncovered the underlying physiological study in mouse sensory system.

Methods

1. Molecular cloning of the TTN family

Primers were designed using the mouse cDNA sequences of *Ttn1-3 (Tmem150a-c)* from the NCBI database (NM_144916.3, NM_177887and NM_182841). Nucleotide fragments of 816, 717 and 750, for *Tmem150a-c* were amplified from cDNA libraries from the kidney, small intestine and epididymis of adult C57BL/6J mice, respectively. Primers used for cloning are listed.

Ttn1 (Tmem150a) forward (5’ ctcgaggccaccatgaccgcct 3’)

reverse (5’ aagcttgatcatggcaatactctcgggag 3’)

restriction sites for XhoI and HindIII

Ttn2 (Tmem150b) forward (5’ ctcgaggccaccatgtggaattacct 3’)

reverse (5’ aagcttgagcacctgtgccatctgta 3’)

restriction sites for XhoI and KpnI

Ttn3 (Tmem150c) forward (5’ ctcgaggccaccatggacgggaagaaat 3’)

reverse (5’ ggtaccctcacctgatccgtctgatattc 3’)

restriction sites for XhoI and KpnI.

Ttn1-3 (tmem150a-c) fragments were cloned into pEGFP-N1 to have fusion proteins

tagged with EGFP. The vector was mutated to include stop codons between the genes and the GFP sequence (pEGFP-N1(STOP)) to express the genes only. The genes were also sub-cloned into pIRES2-AcGFP1 to avoid the GFP fusion effects.

The protein sequence of mouse TTN1 (TMEM150a) is

‘MTAWILLPVSLSAFSITGIWTVYAMAVMNRHVCPVENWSYNESCSPDPAEQGG PKSCCTLDDVPLISKCGTYPPESCLFSLIGNMGAVMVALICLLRYGQLLEQSRHSWI NTTALITGCTNAAGLVVVGNFQVDHAKSLHYIGTGVAFTAGLLFVCLHCVLFYHGATT PLDMAMAYLRSVLAVIAFITLVLSGVFFLHESSQLQHGAALCEWVFVLDILIFYGTFSY EFGTISSDTLVAALQPAPGRACKSSGSSSTSTHLNCAPESIAMI’.

The protein sequence of mouse TTN2 (TMEM150b) is

‘MWNYLSLLPVILFLWAIAGIWIVFAIAVVNGSVDLNEGFPFISICGSYAPQSCIFGQ VLNIGAALTVWICIVRHHQLRDWGVKTWQNQLILWSGILCALGTSIVGNFQDKNQKP THLAGAFLAFILGNLYFWLQFFLSWWVKGLPQPGPHWIKSLRLSLCSLSTILIVAMIV LHALHMRSASAICEWVVAMLLFMLFGFFAVDFSILRGCTLHLHPRLDSSLPQAPSGS PNIQMAQVL’.

The protein sequence of mouse TTN3 (TMEM150c) is

‘MDGKKCSVWMFLPLVFTLFTSAGLWIVYFIAVEDDKILPLNSAARKSGAKHAPYI SFAGDDPPASCVFSQVMNMAAFLALVVAVLRFIQLKPKVLNPWLNISGLAALCLASF GMTLLGNFQLTNDEEIHNVGTSLTFGFGTLTCWIQAALTLKVNIKNEGRRAGIPRVIL

SAVITLCVVLYFILMAQDIHMYAARVQWGLVMCFLAYFGTLAVEFRHYRYEIVCSEYQ

ENFLSFSESLSEASEYQTDQV'.

2. Cell culture and transfection

HEK293T and F11 cells were grown in Dulbecco's modified Eagle medium (DMEM, Life Technologies) supplemented with 10% fetal bovine serum (FBS), 2 mM L-glutamine, 1 mM sodium pyruvate, and 100 U/ml penicillin/streptomycin. Cells were plated on glass coverslips in DMEM supplemented with 10% FBS, 2 mM L-glutamine, and 100 U/ml penicillin/streptomycin in 35 mm dishes.The F11 cells were plated on laminin-coated (2 mg/ml) glass coverslips in DMEM supplemented with 1% FBS, 2 mM L-glutamine, and 100 U/ml penicillin/streptomycin in 35 mm dishes. Half of the medium was replaced every two days.

pIRES2-AcGFP1-TTN1, pIRES2-AcGFP1-TTN2, pIRES2-AcGFP1-TTN3, pEGFP-N1(STOP)-TTN1, pEGFP-N1(STOP)-TTN2, or pEGFP-N1(STOP)-TTN3 vector was transfected for 48 h with Lipofectamine 2000 (Life Technologies) or FuGene (Promega). The pEGFP-N1 vector was used for transfection controls. The *Ttn3* and scrambled siRNA sets were designed, synthesized, and tagged with Cy3 fluorescence by the manufacturer (Bioneer, Seoul, Korea). The siRNA was positioned

at nucleotides 421-439. The sequence is *Tnt3*_siRNA sense 5′-GCUUGUGGAUAGUGUACUU (dTdT)-3′ and antisense 5′-CGAACTCCTATCACATGAA(dTdT)-3′. The Cy3-tagged siRNAs were applied to the cultured DRG cells using Lipofectamine 2000. The siRNA-treated cells were incubated for 48-72 h before use.

3. Isolation of DRG neurons

Primary cultures of DRG neurons were prepared as previously described (Cho et al., 2012). Briefly, thoracic and lumbar DRGs were dissected from 7 to 8-week-old mice and collected in ice-cold medium (DMEM/F12, Life Technologies). Isolated DRGs were then incubated in medium containing 2 mg/ml collagenase IA (Sigma) for 45 min at 37^{o}C. Cells were washed three times with Ca^{2+}- and Mg^{2+}- free Hank's balanced salt solution (Life Technologies). The cells were washed gently two or three times with the culture medium, suspended, and gently triturated with a 1-ml pipette before plating onto round glass coverslips (Fisher). Cells were incubated in culture medium containing DMEM/F12, 10% FBS, 50 ng/ml nerve growth factor (Life Technologies), 5 ng/ml glial cell line-derived neurotrophic factor (Life Technologies), and 100 U/ml penicillin/streptomycin in 95% air/5% CO_2 atmosphere for 48-72 h before use.

4. Channel current recording

Whole-cell currents were recorded using a voltage-clamp technique. Whole cells were formed by breaking the plasma membrane under a glass pipette after gigaseals were made. The resistance of the glass electrodes was 2-3 MΩ. The junctional potentials were adjusted to zero. The holding potential was set at -60 mV. Currents were amplified with Axopatch200B (Molecular Devices), filtered by 0.5 kHz, digitized at a sampling rate of 5 kHz with Digidata 1440 (Molecular Devices), and stored in a computer. The stored currents were later analyzed using the pClamp software (version 10.0, Molecular Devices).

For DRG neuron recordings, the pipette solution contained 130 mM KCl, 2 mM $MgCl_2$, 5 mM EGTA, 10 mM HEPES, 2 mM Mg-ATP, 0.2 mM Na-GTP, and 20 mM D-mannitol. The pH of the solution was adjusted to 7.2 with KOH. The bath solution contained 130 mM NaCl, 5 mM KCl, 1 mM $CaCl_2$, 2 mM $MgCl_2$, 10 mM HEPES, and 10 mM D-mannitol at pH 7.2, adjusted with NaOH. For recording currents in cell lines, the pipette solution contained 130 mM CsCl, 2 mM $MgCl_2$, 10 mM HEPES, 2 mM Mg-ATP, 0.2 mM Na-GTP, and 25 mM D-mannitol. The pH was adjusted to 7.2 with CsOH. For the cation selectivity experiment, the pipette solution contained 150 mM CsCl and 10 mM HEPES at pH 7.2, adjusted with CsOH. The bath solution contained 150 mM NaCl, 150 mM KCl, 150 mM NMDG-Cl, 100 mM $CaCl_2$, or 100 mM $MgCl_2$ and 10 mM

HEPES. The pH was adjusted to 7.2 with NaOH, KOH, or CsOH for divalent cation solutions. For the anion/cation permeability experiments, the pipette solution contained 70 mM NaCl whereas the bath solution contained 210 mM NaCl. The osmolarity of all of the solutions was adjusted to 290 mOsm by adding D-mannitol. The P_{Cl}/P_{Na} of each mutant was obtained by measuring the reversal potential of the steady-state current of each mutant using the Goldman-Hodgkin-Katz equation (Arreola and Melvin, 2003).

To determine the current-voltage relationships, voltage ramps from -80 to +80 mV were applied for 150 ms to whole cells during 600 ms mechanical stimulation. For blocker experiments, 50 μM chloropromazine (Sigma), 10 μM HC-030031 (Sigma), 30 μM ruthenium red (Sigma), 30 μM FM1-43 (Biotium), 2.5 μM GsMTx-4 (Tocris), or 30 μM $GdCl_3$ (Sigma) was added to the bath solution. To get a dose-response curve for the Gd^{3+} inhibition, the normalized current (I/I_{MAX}) was fitted to the Hill equation, I/I_{MAX} (%) = $[1 + (K_D/[Gd^{3+}])^n]^{-1}$, where K_D represents the half-maximal effect of Gd^{3+} and **n** is the Hill coefficient.

5. Mechanical stimulation

A fire-polished glass electrode (tip diameter ~3-4 μm) was positioned at an angle of ~50° to the cell surface. The probe was moved by a micromanipulator (Nano-controller NC4, Kleindiek Nanotechnik, Germany). The movement of the probe was controlled either by a joystick or by a computer. The initial position of the probe on the cell surface was determined by looking at the indentation of the cell surface through a microscope. Then, 1.0 μm retraction was made, which was considered to be the initial point of all mechanical stimuli. From the initial position, the mechanical steps were made by moving the glass probe forward from 2.5 - 7.2 μm with 0.42 μm increments. The typical duration of the mechanical stimulation was 100 or 600 ms.

6. Recording of MS afferent activity

The muscle-nerve ex vivo preparation and recording muscle fiber activity were described by others (Franco et al., 2014; Wilkinson et al., 2012). Briefly, mice were deeply anesthetized with isoflurane, decapitated immediately, and skinned. EDL muscle and the peroneal nerve attached to it were isolated in the chilled (4°C) solution containing 128 mM NaCl, 1.9 mM KCl, 1.2 mM KH_2PO_4, 26 mM $NaHCO_3$, 0.85 mM $CaCl_2$, 6.5 mM $MgSO_4$, and 10 mM glucose (pH 7.4). The isolated EDL muscle-nerve

preparation was mounted into a tissue bath filled with the oxygenated solution containing 123 mM NaCl, 3.5 mM KCl, 0.7 mM $MgSO_4$, 1.7 mM NaH_2PO_4, 2.0 mM $CaCl_2$, 9.5 mM $NaC_6H_{11}O$, 5.5 mM glucose, 7.5 mM sucrose, and 10 HEPES (pH 7.4). Thin silk sutures were used to tie both ends of the EDL muscle to a micrometer and a force transducer for adjusting muscle stretch and measuring force. The output signal of the force transducer was amplified to report the magnitude of muscle stretch, which was well correlated with force applied to the muscles. A suction electrode was made with a glass pipette whose tip diameter was 70 μm. The suction electrode was filled with the bath solution. The free end of the peroneal nerve was suctioned into the electrode. To identify MS afferents, suctions were repeated until neuronal activities were observed during muscle stretches. Stretches for 5 sec in length of 2 mm were repeated three times and two more stretches with stretch lengths of 1 and 3 mm. Electrical signals in the suction electrode were amplified with ISO-80 (World Precision Instruments), filtered by 1 kHz, digitized at a sampling rate of 10 kHz with Digidata 1322 (Molecular Devices), and stored in a computer. The stored traces were later analyzed using the pClamp software (version 10.0, Molecular Devices). Spikes above one standard deviation of the noise were counted as action potentials of the nerve.

7. Phylogenetic Analysis

Multiple sequence alignments and the phylogenetic dendrogram were performed using the CLUSTALW program. GenBank accession IDs are shown in Table.

8. Antibody production

A peptide spanning the c-terminus of mouse TTN3 (211~249 a.a: LAVEFRHYRYEIVCSEYQENFLSFSESLSEASEYQTDQV) was synthesized and immunized three times to a rabbit (AbFrontier Co, Seoul, Korea). The immunized rabbit serum was purified with protein A-Sepharose column chromatography and with antigen-specific affinity column. The specificity of purified antibody was confirmed by ELISA.

9. Animals and *Ttn3* KO mouse

Mice were used under protocols approved by the Institute of Laboratory Animal Resources of the Seoul National University. Typically, 7 to 8-week-old mice were used for all experiments.

The mutant mouse was generated by trans-NIH Mouse Initiative Knockout Mouse

Project (KOMP; www.nih.gov/science/models/mouse/knockout/). Briefly, *LacZ* was inserted between exon 5 and 6 of the *Ttn3* locus with stop codon, which resulted in the expression of truncated *Ttn3* and *LacZ* fusion protein. The $Ttn3^{+/-}$ mice were crossed with wild type mouse to produce additional $Ttn3^{+/-}$ mice. These $Ttn3^{+/-}$ mice were then crossed each other to further produce $Ttn3^{-/-}$ mice.

10. Immunohistochemistry

Mouse EDL muscles were fixed in 4% polyformaldehyde for 24 h, paraffin-embedded, and cut in 5-μm with a vibratome. Each section was incubated with 3% H_2O_2 in methanol for 30 min to quench endogenous peroxidase activity. Tissue sections were dehydrated with graded alcohols and exposed to 10 mM sodium citrate for antigen retrieval. The sections were blocked with phosphate buffered saline (PBS) containing 5% normal goat serum and 0.3% Triton X-100 for 1 h at room temperature and then incubated with anti-TTN3 (1:100) antibody diluted in PBS containing 1% bovine serum albumin and 0.3% Triton X-100 overnight at 4°C. The sections were subsequently washed three times, incubated for 1 h with HRP-conjugated secondary antibody, incubated with 3,3′-diaminobenzidine tetrahydrochloride (DAB, Sigma) after

wash, and immediately washed under tap water after the color development. Slides were stained with hematoxylin and eosin.

11. Immunofluorescence

Immunofluorescent staining of tissue sections were performed as previously described (Cho et al., 2012). Briefly, DRGs or EDL muscles were isolated from adult mice (7-8 weeks) and sectioned on a cryostat at 10 μm and fixed in 4% polyformaldehyde. Sections were washed and incubated with blocking buffer (10% (wt/vol) goat serum or 4% bovine serum albumin in PBS with 0.1% Triton-X or 0.1% Triton-X for muscles) for 1 hour. Polyclonal TTN3 (1:700), TRPV1 (AB5566, Millipore, 1:500), or NFM (sc-51683, SantaCruz, 1:500) antibody was incubated with samples in the blocking buffer overnight at 4°C or 48 hours at 4°C for muscles. Samples were then washed and incubated with Alexa Fluor 546–conjugated goat anti-rabbit (A11010, Life Technology, 1:500) or Alexa Fluor 488-conjugated goat anti-guinea pig (AP193F, Invitrogen, 1:800) or Alexa Fluor 488-conjugated goat anti-chicken (A11039, Invitrogen, 1:800) or isolectin B4 (I21411, Invitrogen, 20 μg/ml) at room temperature for 1 h. Nucleus was stained using Hoechst 33342 for 10 min (H3570, Thermofisher Scientific,

1:2000) The sections were imaged with a confocal microscope (LSM700, Carl Zeiss).

12. Western blot

M-PER (Mammalian Protein Extraction Reagent, Thermo) and a complete protease inhibitor cocktail (Roche) were added to F11 cell cultures to lyse cells. Lysates were then scraped off and centrifuged at 13,000 rpm for 10 min to obtain the supernatant of cell extracts. The supernatant was then denatured at 100°C and separated on a 4 - 12% NuPAGE®Bis-Tris gel (Invitrogen) and transferred onto PVDF membranes. After blocking with 5% skim milk, the membranes were incubated with TTN3 (1:1000) or β-actin (1:5000, Sigma, A2066) antibody overnight at 4°C. The membranes were washed three times with Tris-buffered saline supplemented with 0.05% Tween 20. The membranes were incubated with anti-rabbit IgG-horseradish peroxidase secondary antibody (1:2000, Cell signalling, 7074S). The bands were visualized using the enhanced chemi-luminescence reagent (Pierce).

13. Inverted screen test

Mice are allowed to grip a welded wire mesh (560 mm x 510 mm) composed of

small squares (11.5 mm x 11.5 mm, 0.8 mm in diameter) by their all paws (Cassani et al., 2015; Jeyakumar et al., 1999). The mesh was then slowly inverted and held steadily 30 cm above a soft surface. Hanging time was measured until mice fell down. The cut-of-time was set at 600 sec.

14. Beam walking test

The beam walking test for WT and Ttn3 KO mice were performed as described elsewhere (Carter et al., 2001; Chort et al., 2013; Yokoi et al., 2012). Briefly, mice were trained to travel a 12-mm wide plastic beam (80-cm long, 50-cm high) for 3 times a day for two days, followed by 6 mm wide beam for 3 times. At the end of the bar, there was a dark cage so that mice were let to cross the beam to hide themselves. On the 3rd day, mice were let to travel the 6-mm wide beam. Movements of mice were recorded by video. Traveling time and the number of foot slips were measured.

15. Catwalk Gait analysis

Mouse gait was analyzed as described elsewhere (Cote et al., 2012; Encarnacion et al., 2011; Hamers et al., 2006; Lucas et al., 2014). Briefly, gait analysis was

assessed by the CatWalk system (Noldus Information Technology). The apparatus was consisted of a 1.3-m long glass floor under which a light source illuminated the floor in a dark environment. When a mouse was walking through the floor, the plantar regions of the mouse paws glowed because of the light deflection. The foot prints were then recorded by a video camera and stored in a computer. Mice were subjected to have three successive runs. A mouse run was considered successful if a mouse walked the walkway in 5 sec. After identification and labeling of each footprint, gait parameters were analyzed with Catwalk XT software. All parameters of a mouse represented as an average of three trials. ***Average speed*** refers to the velocity of a mouse. ***Swing speed*** refers to the velocity of the moving limb during the swing phase. ***Stride length*** represents the length of the stride cycle. ***Regularity index*** refers to the percentage of normal step-sequence patterns relative to the total number of paw placements. ***Phase dispersion*** is the percentage of initial contact of one paw (target paw) relative to the stride cycle of another paw (anchor paw).

16. Statistical analysis

Data in the figures were shown as mean ± S.E.M. To compare two means, unpaired two-tailed Student's *t*-test was used. One-way or two-way ANOVA was used to compare multiple means.

Protein Acc.	Gene	*Organism*	
NP_001073975.1	*Ttn3*	*H. sapiens*	Human
NP_878261.1	*Ttn3*	*M. musculus*	mouse
NP_001101824.1	*Ttn3*	*R. norvegicus*	rat
XP_420558.4	*Ttn3*	*G. gallus*	chicken
XP_005155606.1	*Ttn3*	*D. rerio*	zebrafish
XP_002936503.1	*Ttn3*	*X. tropicalis*	frog
XP_007065696.1	*Ttn3*	*C. mydas*	turtle
XP_003985286.1	*Ttn3*	*F. catus*	cat
NP_001026908.1	*Ttn1*	*H. sapiens*	human
NP_659165.1	*Ttn1*	*M. musculus*	mouse
NP_620807.1	*Ttn1*	*R. norvegicus*	rat
XP_421633.3	*Ttn1*	*G. gallus*	chicken
NP_001038875.1	*Ttn1*	*D. rerio*	zebrafish
NP_001016894.1	*Ttn1*	*X. tropicalis*	frog
XP_007069920.1	*Ttn1*	*C.mydas*	turtle
XP_003984259.1	*Ttn1*	*F. catus*	cat
NP_001268940.1	*Ttn2*	*H. sapiens*	human
NP_001136264.1	*Ttn2*	*M. musculus*	mouse
NP_001100946.1	*Ttn2*	*R. norvegicus*	rat
NP_001032458.1	*Ttn2*	*D. rerio*	zebrafish
NP_001015997.1	*Ttn2*	*X. tropicalis*	frog
XP_003997471.1	*Ttn2*	*F. catus*	cat

Table. GenBank accession IDs from phylogenetic analysis.

Results

1. Cloning of Tentonin 3

To find MA channels with slow inactivation kinetic, we performed a bioinformatic investigation (Coste et al., 2010; Yang et al., 2008). We first screened DNA chips (Agilent) after hybridization with RNAs isolated from human DRG cells and six human cell lines; human embryonic kidney (HEK) 293T, Henrietta Lacks (HeLa), retinal pigment epithelium (RPE), human keratinocyte (HaCaT), hepatocellular carcinoma (HepG2), and human cervical carcinoma (SiHa) cells. We expected that slowly adapting (SA) MA channels would be found mainly in the DRG neurons. Therefore, we searched for genes in the six human cell lines whose hybridization intensities were less than that of DRG cells. In addition, we filtered out genes of known function or genes encoding five or less transmembrane domains. We then transfected Cy3-tagged siRNAs of the selected candidate genes into isolated DRG neurons from adult mice and tested if they showed a reduction in the SA currents in response to mechanical steps. We found that knockdown of one gene, *Tmem150c*, showed a marked reduction in the amplitude of the SA currents as well as in population of SA type neurons (Fig. 5,6). We renamed this gene ‘Tentonin 3’ after the Greek ‘**tentono**,

τεντωνω', meaning 'to stretch'.

2. TTN3 is required for slowly adapting MA currents in DRG neurons

Mechanical activation of dissociated DRG neurons induced three distinct types of MA currents, rapidly adapting (RA), intermediately adapting (IA), and SA, with τ_i of < 10 ms, 10 < τ_i < 30 ms, and > 30 ms, respectively (Coste et al., 2010; Hao and Delmas, 2010) (Fig. 5). The proportions of RA, IA, and SA type control (transfected with scrambled siRNA) DRG neurons (236 cells) were 41%, 25%, and 22%, respectively. In contrast, when Cy3-tagged *Ttn3* siRNA was transfected to DRG neurons, the proportion of cells with SA MA currents was reduced to 10% (Fig. 6A,C). In order to see a clearer phenotype, *Ttn3* knockout (KO) mice were generated (Fig. 7). The proportion of SA type neurons was dramatically reduced to 4% in *Ttn3* KO DRG neurons (Fig. 6C). Notably, we could not observe SA currents that had inactivation time constant (τ_i) longer than 80 ms in *Ttn3* KO DRG neurons (Fig. 6B). Thus, these results indicate that TTN3 is essential for SA currents in DRG neurons.

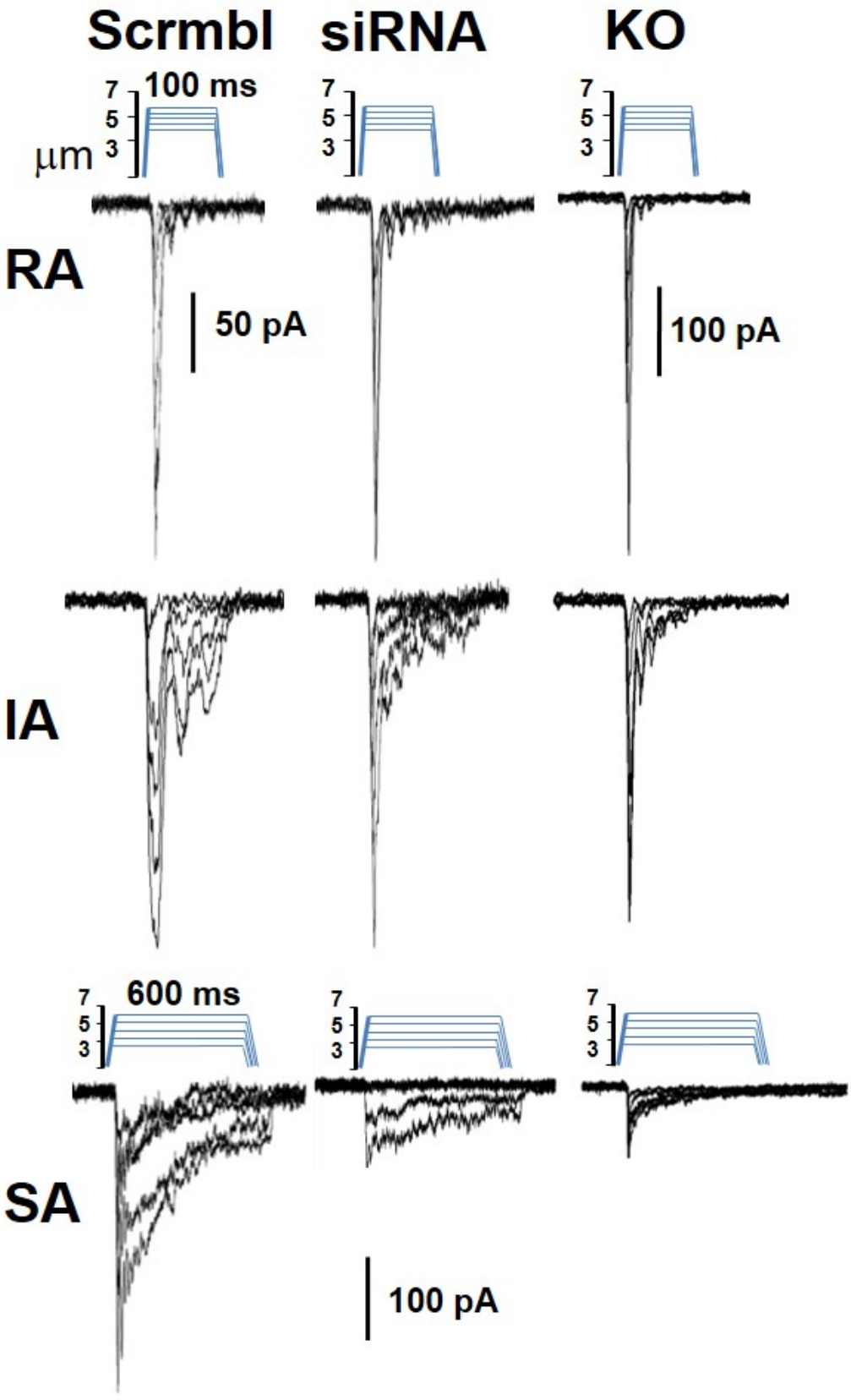
Scrmbl
siRNA
KO
100 ms
7
5
3
μm
RA
50 pA
100 pA
IA
600 ms
SA
100 pA

Figure 5. Representative MA currents in DRG neurons.

Representative traces of three types of MA currents in DRG neurons transfected with scrambled siRNA (Scrmbl) or Ttn3-siRNA (siRNA), or isolated from *Ttn3* KO (KO) mice. The DRG neurons were stimulated by mechanical steps with 0.42 mm or 0.84 mm increments for 100 or 600 ms.

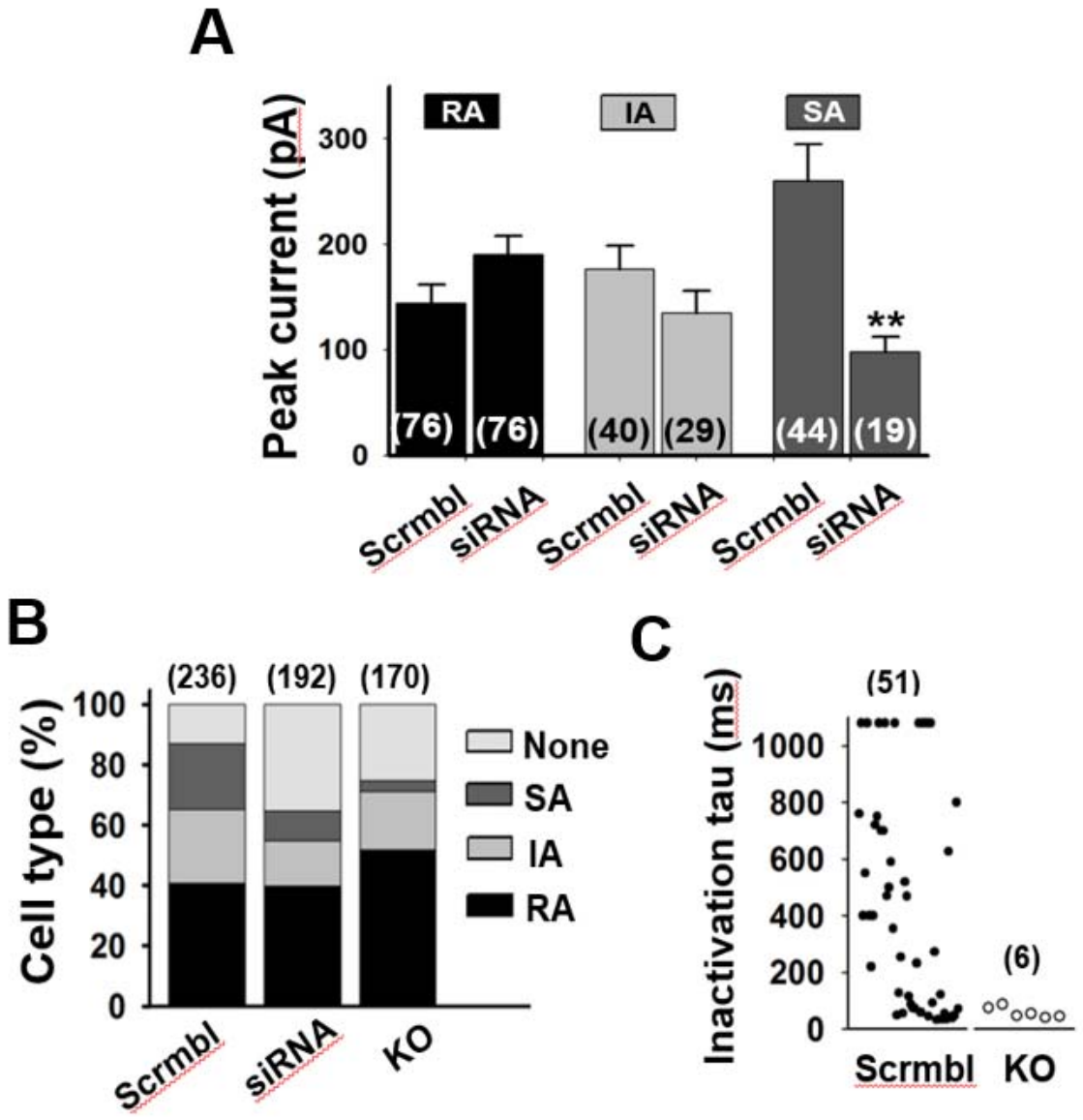
A
RA
IA
SA
Peak current (pA)
300
200
100
0
(76)
(76)
(40)
(29)
(44)
(19)
**
Scrmbl
siRNA
Scrmbl
siRNA
Scrmbl
siRNA
B
(236)
(192)
(170)
Cell type (%)
100
80
60
40
20
0
None
SA
IA
RA
Scrmbl
siRNA
KO
C
(51)
Inactivation tau (ms)
1000
800
600
400
200
0
(6)
Scrmbl
KO

Figure 6. Summary of MA currents in *Ttn3* deficient DRG neurons

A) Distribution of the inactivation time constant (t_i) of SA type MA currents in DRG neurons transfected scrambled siRNA (●) or isolated from *Ttn3* KO (○) mice.

B) Peak currents of DRG neurons activated by 6.3 mm mechanical steps after being transfected with scrambled (Scrmbl) or *Ttn3* siRNA. The DRG neurons were classified by the inactivation kinetics of the MA currents. Inactivation time constants (t_i) for RA, IA, and SA MA currents were < 10 ms, 10 < t_i < 30 ms, and > 30 ms, respectively. **p < 0.01, Student's *t*-test.

C) Histogram of cell type among the DRG neurons. The DRG neurons were classified by the inactivation kinetics of the MA currents. Inactivation time constants (t_i) for RA, IA, and SA MA currents were < 10 ms, 10 < t_i < 30 ms, and > 30 ms, respectively.

Figure 7. Generation of TTN3 KO mouse

Vector construct for gene targeting. Exon 6 in the *Ttn3* locus is flanked with two *loxP* sites preceded by a FRT-flanked neo and lacZ cassette.

3. Activation by mechanical stimulation

Tentonin 3 (TTN3) is a relatively small protein with 249 amino acids, predicted to have 6 transmembrane domains (Fig. 8). A search for orthologs in the animal kingdom revealed that only vertebrates (*phylum chordata*) have this gene family. The *Ttn* genes were not found in the lower phyla of the animal kingdom or in plants (Fig. 9). TTN3 appeared to be less related to the other two paralogs, sharing 26.5% and 28.1% sequence identity with TTN1 and TTN2, respectively. In contrast, mouse TTN3 had 96% and 99% amino-acid sequence similarity with its human and rat orthologs, respectively.

Majority of TTN3 was observed to be targeted to the plasma membrane when overexpressed heterologously in HEK293T cells (Fig. 10). To test its mechanosensitivity, whole-cell currents were recorded from various cell lines transfected with pIRES2-AcGFP1-TTN3. The plasma membrane surface of TTN3-expressing cells was distended with a piezo-electrically driven glass probe. When mechanical steps were applied to the cell, robust currents were activated in HEK293T cells (Fig. 11). After the rapid activation, these currents showed rapid inactivation followed by slowly inactivating MA currents, which persisted as long as the mechanical stimuli were sustained. When the mechanical steps were withdrawn, the currents were deactivated, with residual currents persisting for more than several seconds (Fig. 11-

13). The mean current was 975.7 ± 113.8 pA in *Ttn3*-transfected HEK293T cells (Fig. 11B). The mechanical steps evoked MA currents greater than 200 pA in 34 out of 66 *Ttn*3-transfected HEK293T cells (52%). Only 7 out of 45 (16%) *Gfp*-transfected control cells responded to the mechanical steps with small current amplitudes (82.7 ± 12.6 pA, n =7) and fast inactivation kinetics in consistent with previous research (Coste et al., 2010).

Two homologs, TTN1 (TMEM150A) and TTN2 (TMEM150B), also showed MA currents when expressed in HEK293T cells, but to a much smaller magnitude (Fig. 11B). The inactivation time constant (τ_i) was 286.1 ± 41.1 ms (n = 7). The steady-state currents at 600 ms mechanical stimulus were about 52.5% of the peak currents in TTN3/HEK293T cells. Due to the slow inactivation time constants (> 30 ms), these TTN3-dependent MA currents were classified as the SA mechanotransduction group observed in DRG neurons (Hao and Delmas, 2010).

F11 is a cell line hybridizing between a mouse neuroblastoma, N18TG-2, and rat DRG neurons (Ghil et al., 2000). F11 cells have a round and big cell soma like DRG neurons so that it is easy to apply mechanical step stimuli. Mechanical activation on F11 cells transfected with *Ttn3* also induced MA currents (1,958 ± 194 pA, n = 33) with slow inactivation kinetics (Fig.12A). Mechanical activation on control F11 cells induced small MA currents (187.9 ± 22.2 pA, n = 19). The mechanical steps evoked MA

currents (>200 pA) in 33 out of 41 (80%) *Ttn*3-transfected F11 cells. When mechanical steps with variable distances were applied to the surface of the *Ttn*3-transfected F11 cells, graded MA currents were observed (Fig. 12A). The mechanical steps also induced large MA currents with slow inactivation kinetics in HeLa cells transfected with *Ttn3* (Fig. 13).

Taken together, TTN3 is activated by mechanical steps when expressed heterologously in various cell types.

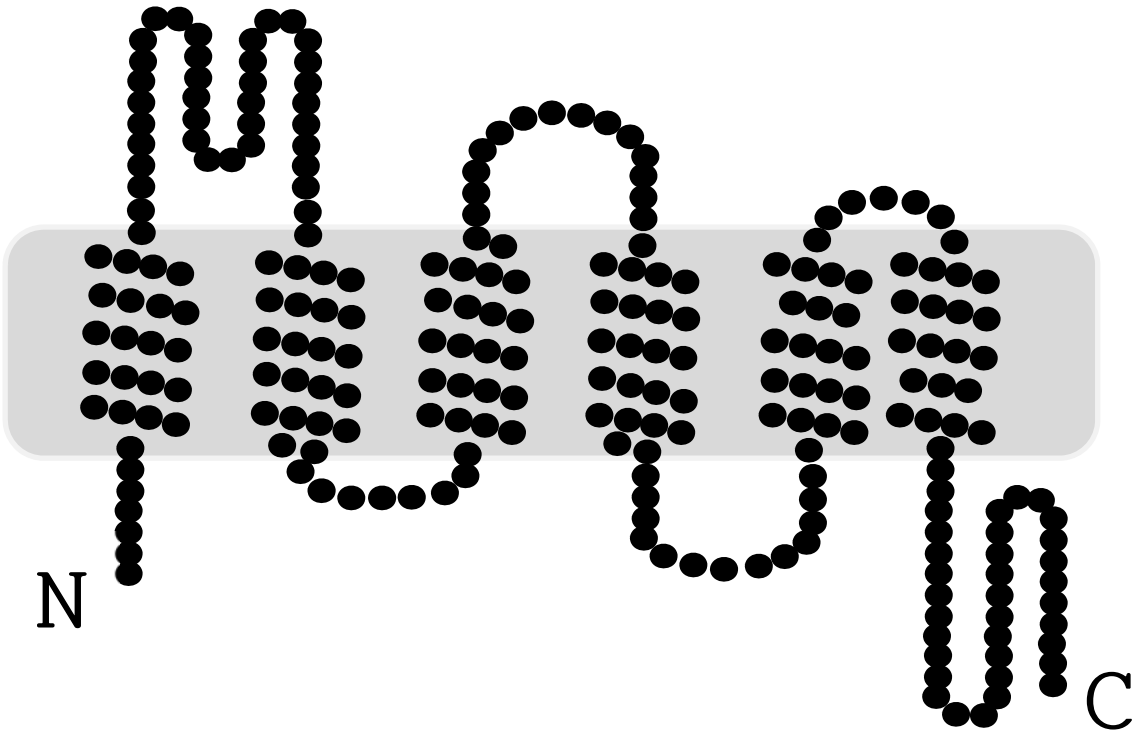

Figure 8. A putative topology of TTN3

TTN3 was predicted by the TMHMM program. Each dot represents an amino acid in mouse TTN3.

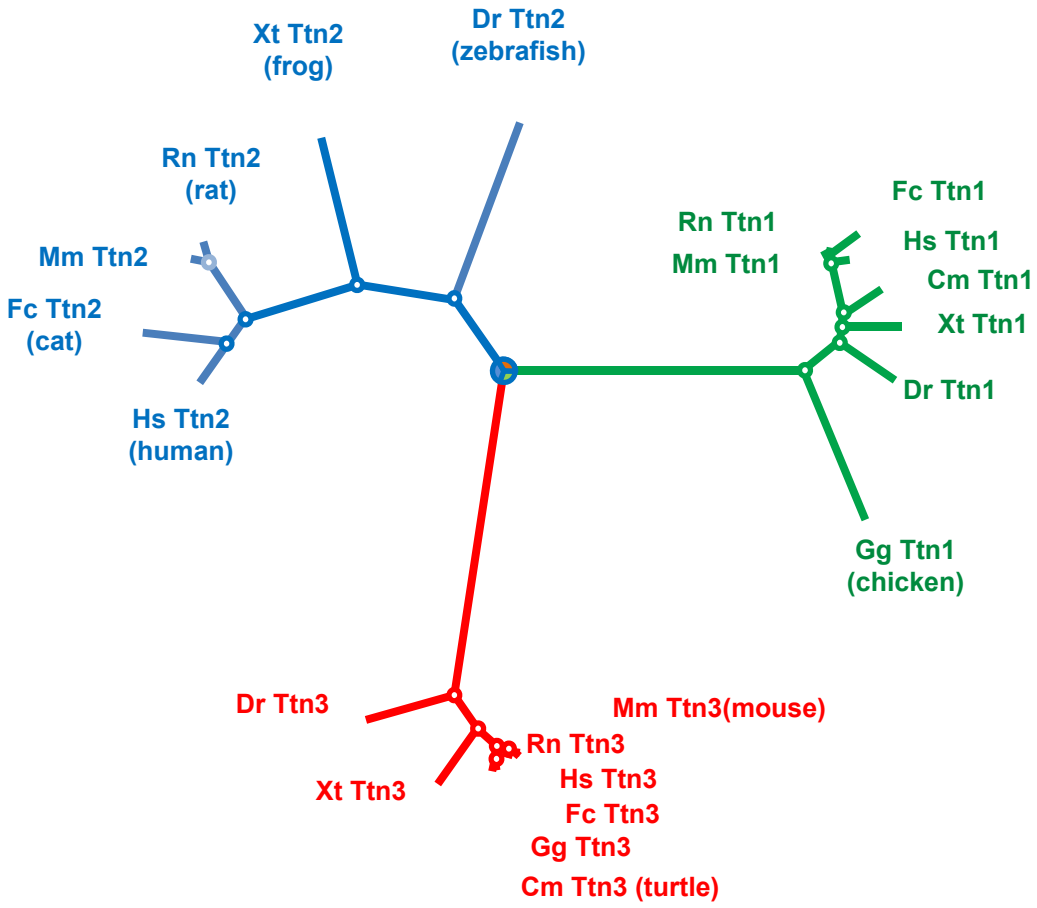

Figure 9. Phylogenetic dendrogram

A phylogenetic tree of the Ttn gene family among different species in vertebrates (phylum Chordata). The sequence alignment and dendrogram were drawn using the CLUSTALW program. Cm, Chelonia mydas; Dr, Danio reiro; Fc, Felis catus; Gg, Gallus gallus; Hs, Homo sapiens; Mm, Mus musculus; Rn, Rattus norvegicus; Xt, Xenopus tropicalis.

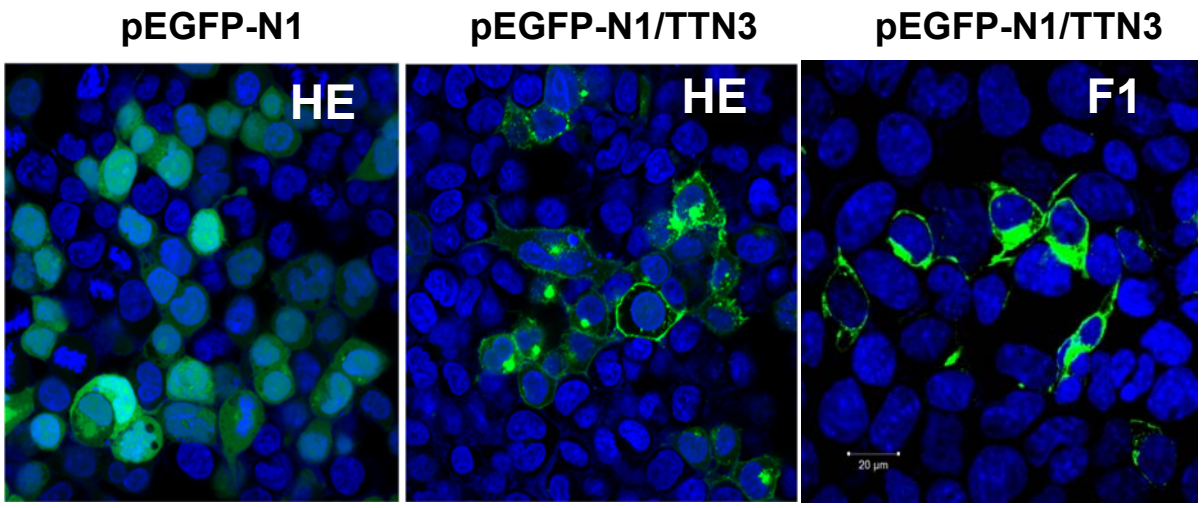

Figure 10. The localization of TTN3 when overexpressed in HEK293T and F11 cells.

A fusion protein, TTN3-GFP was overexpressed in HEK293T or F11 cells and stained with Hoechst 33342. GFP alone was also overexpressed in HEK283T cells for comparison (right panel).

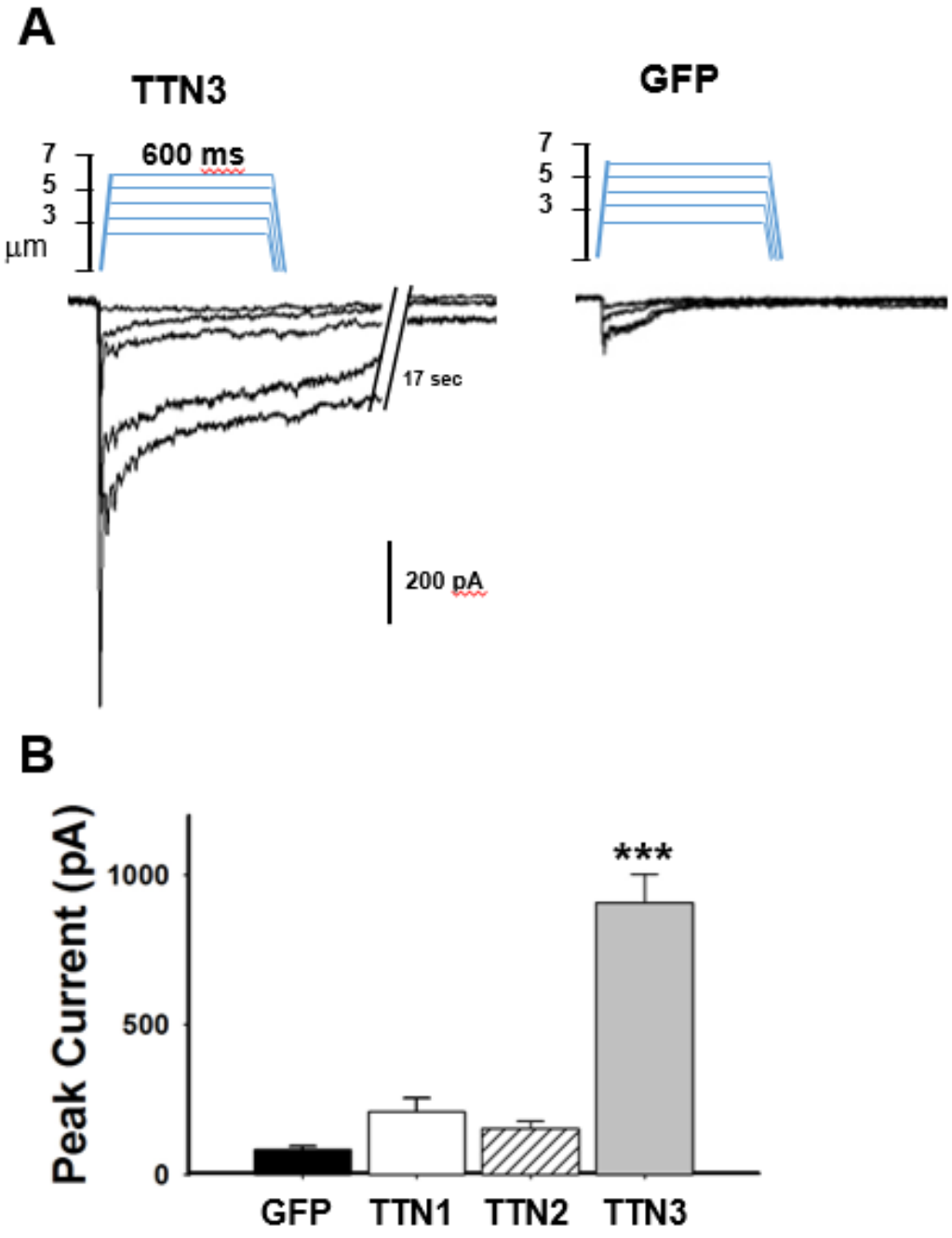
A
TTN3
GFP
600 ms
7
5
3
µm
17 sec
200 pA
B
Peak Current (pA)
1000
500
0
***
GFP
TTN1
TTN2
TTN3

Figure 11. TTN3 induces mechanically-activated (MA) currents in HEK293T cell.

A) Representative traces of the currents activated by the mechanical steps in *Ttn3*- and *Gfp*-transfected HEK293T cells. After forming a whole cell, mechanical steps of 600 ms duration were applied to the surface. E_{hold} = -60 mV.

B) Average peak amplitudes of MA currents activated by a 5.0 mm mechanical step in *Ttn1*-, *Ttn2*-, *Ttn3*-, *Gfp*-transfected HEK293T cell.

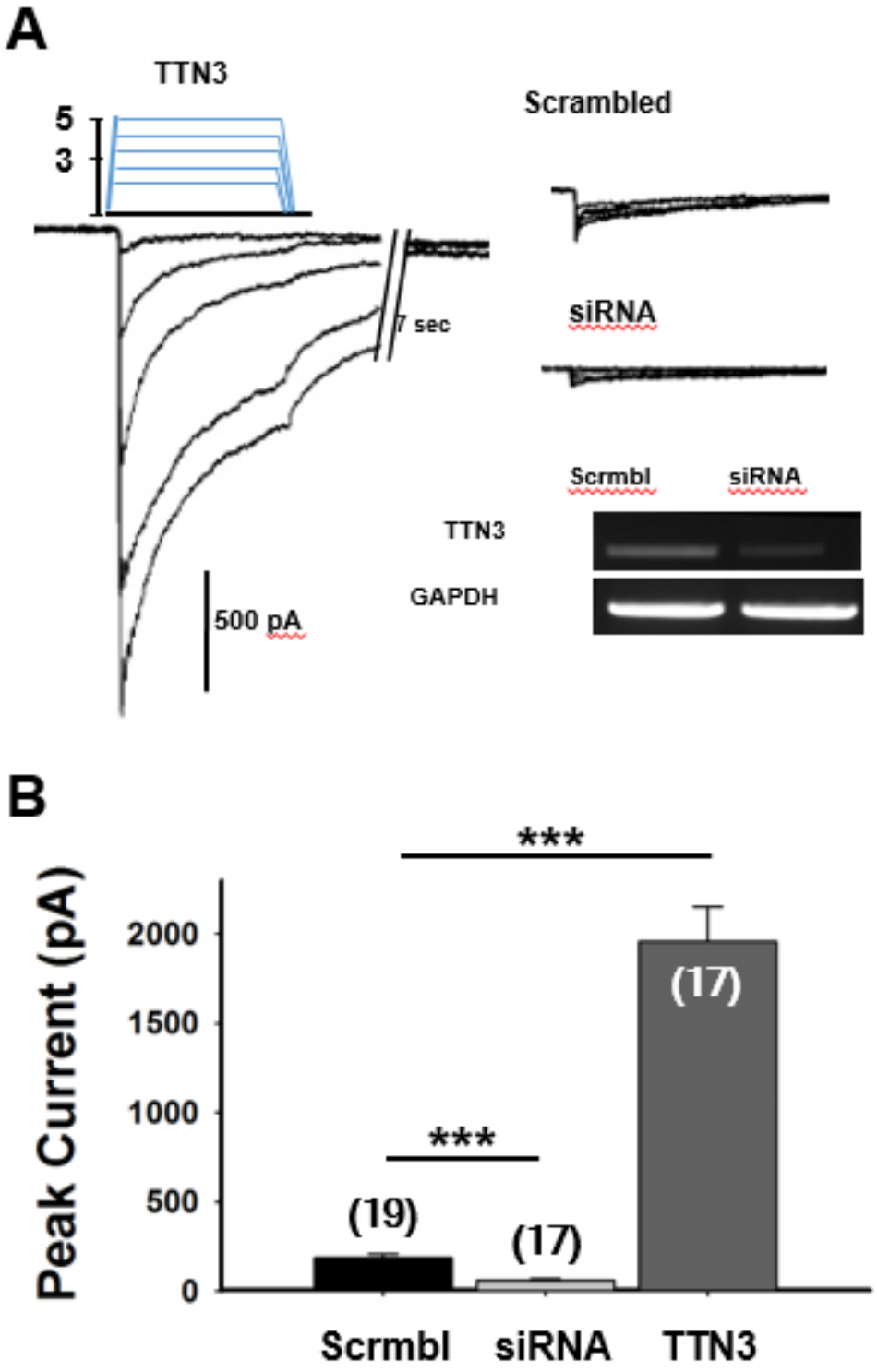
A
TTN3
5
3
7 sec
500 pA
Scrambled
siRNA
Scrmbl
siRNA
TTN3
GAPDH
B
Peak Current (pA)
2000
1500
1000
500
0
***
***
(19)
(17)
(17)
Scrmbl
siRNA
TTN3

Figure 12. TTN3 induces mechanically-activated (MA) currents in F11 cell.

A) Representative traces of MA currents in *Ttn3*-, scrambled siRNA (Scrmbl)-, and *Ttn3*-siRNA-transfected (siRNA) F11 cells. Inset, gene expression of *Ttn3* in Scrmbl and siRNA-transfected F11 cells (28 PCR cycles, 48 h after transfection). Glyceraldehyde-3-phosphate dehydrogenase (GAPDH) was used as a reference.

B) Average peak amplitudes of MA currents activated by a 5.0 mm mechanical step in scrambled siRNA (Scrmbl), *Ttn3*-siRNA (siRNA), and *Ttn3*-transfected F11 cells. Bars represent S.E.M. The numbers in brackets represent the number of cells tested. ***$p < 0.001$, one-way ANOVA, Tukey's post-hoc test.

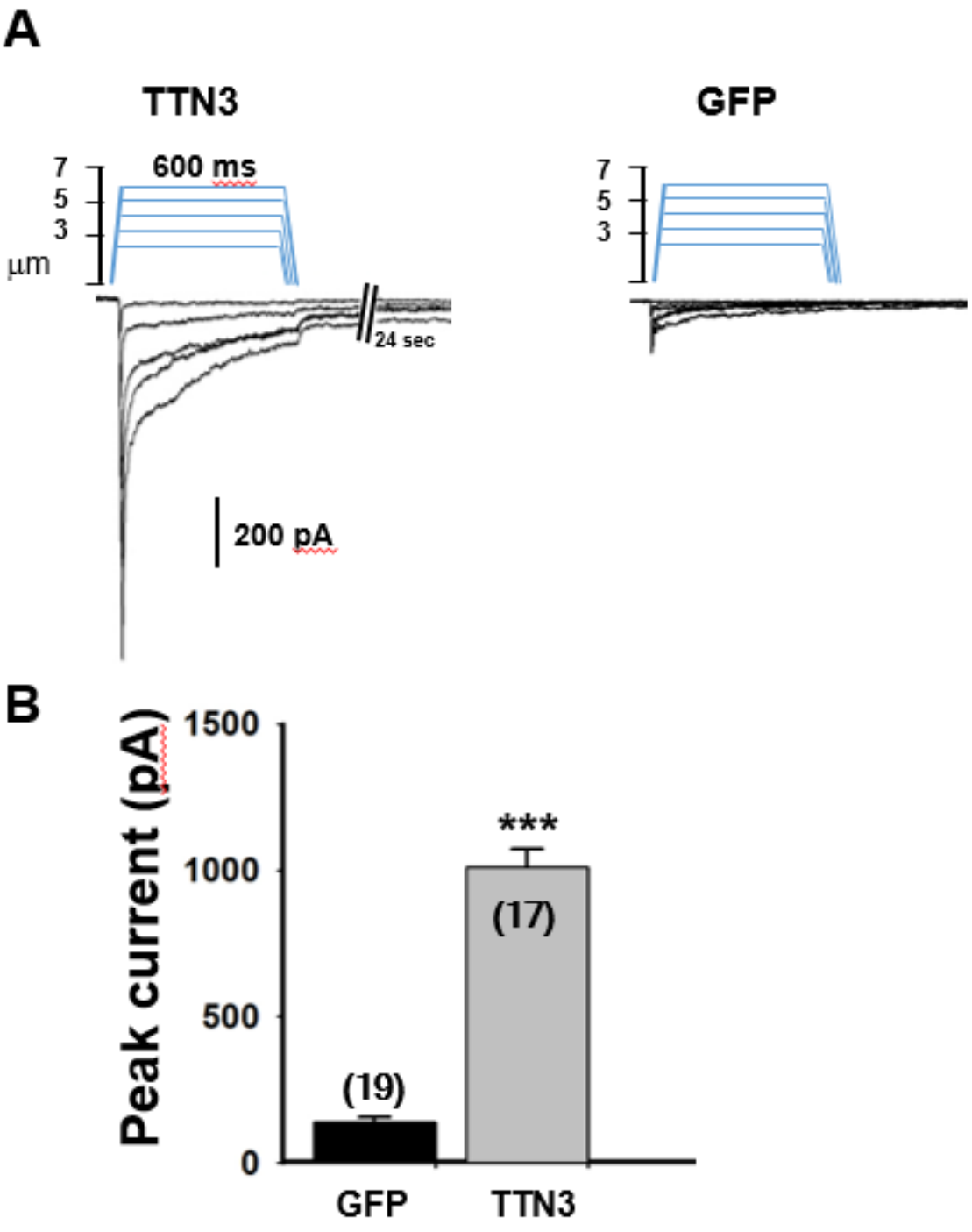
A
TTN3
GFP
600 ms
7
5
3
µm
24 sec
200 pA
B
Peak current (pA)
1500
1000
500
0
***
(17)
(19)
GFP
TTN3

Figure 13. TTN3 induces mechanically-activated (MA) currents in HeLa cell.

A) Representative traces of the currents activated by the mechanical steps in *Ttn3*- and *Gfp*-transfected HeLa cells. After forming a whole cell, mechanical steps of 600 ms duration were applied to the surface. E_{hold} = -60 mV.

B) Average peak amplitudes of MA currents activated by a 5.0 mm mechanical step in *Ttn1*-, *Gfp*-transfected HeLa cell.

4. Biophysical property

The steady-state currents at 600 ms mechanical stimulus of the peak currents (I_{SS}/I_{MAX}) were about 52.5% in TTN3/HEK293T cells and 47.8% in TTN3/F11 cells (Fig. 14A).

The half-maximal distance for activating TTN3 was 4.8 ± 0.2 μm (n = 6), which was similar to that for human Piezo1 (4.7 ± 0.3 μm, n = 6) expressed in F11 cells (Fig.14B). However, the threshold distance (3.2 ± 0.1 μm, n = 6) for activating TTN3 was significantly larger than that for Piezo1 (2.3 ± 0.2 μm, n = 6, $p < 0.01$, Student's *t*-test).

The inactivation rates of MA currents in TTN3-expressing cells were best fitted to mono- or bi-exponential curves (Fig. 15). The inactivation time constant (τ_i) of mono-exponential curves was 286.1 ± 41.1 ms (n = 7).

The steady-state currents of TTN3 induced by mechanical steps of different durations persisted as long as the mechanical stimuli were maintained up to 1,000 ms (Fig. 16A). In addition, MA current followed the sinusoidal steps applied after a 200 ms conditioning step (Fig. 16B).

To test the slow-inactivating kinetics further, a two-step mechanical stimulus protocol was used, consisting of 100 ms conditioning steps with indentations of 2.9 to 4.6 μm with 0.42 μm increments, followed by a 4.6-μm test step (Fig. 17A). Even though the magnitudes of conditioning steps varied, the peak or steady-state MA

currents at the test steps did not change (Fig. 17B). Thus, a large portion of the MA current still persisted at the test step. These results indicate that some TTN3 are still active even after prolonged mechanical stimuli, which is a property of SA currents found in DRG neurons (Hao and Delmas, 2010).

The current-voltage relationship of the steady-state current was obtained to measure the reversal potential (Fig. 18). The TTN3 MA current was cationic with a reversal potential of 6.7 ± 0.7 mV (n = 9) in 150 mM CsCl and 150 mM NaCl for pipette and bath solutions, respectively. Judging by the reversal potentials when the bath solution was changed to 150 mM NaCl, 150 mM KCl, 100 mM $CaCl_2$, or 100 mM $MgCl_2$, the permeability ratios (P_x/P_{cs}) between Na^+, K^+, Mg^{2+}, and Ca^{2+} and Cs^+ were 1.31 ± 0.04 (n = 9), 1.24 ± 0.05 (n = 6), 1.41 ± 0.15 (n = 6), and 2.01 ± 0.11 (n = 8), respectively (Fig. 19). Thus, TTN3 is a nonselective cationic channel with high permeability to Ca^{2+}.

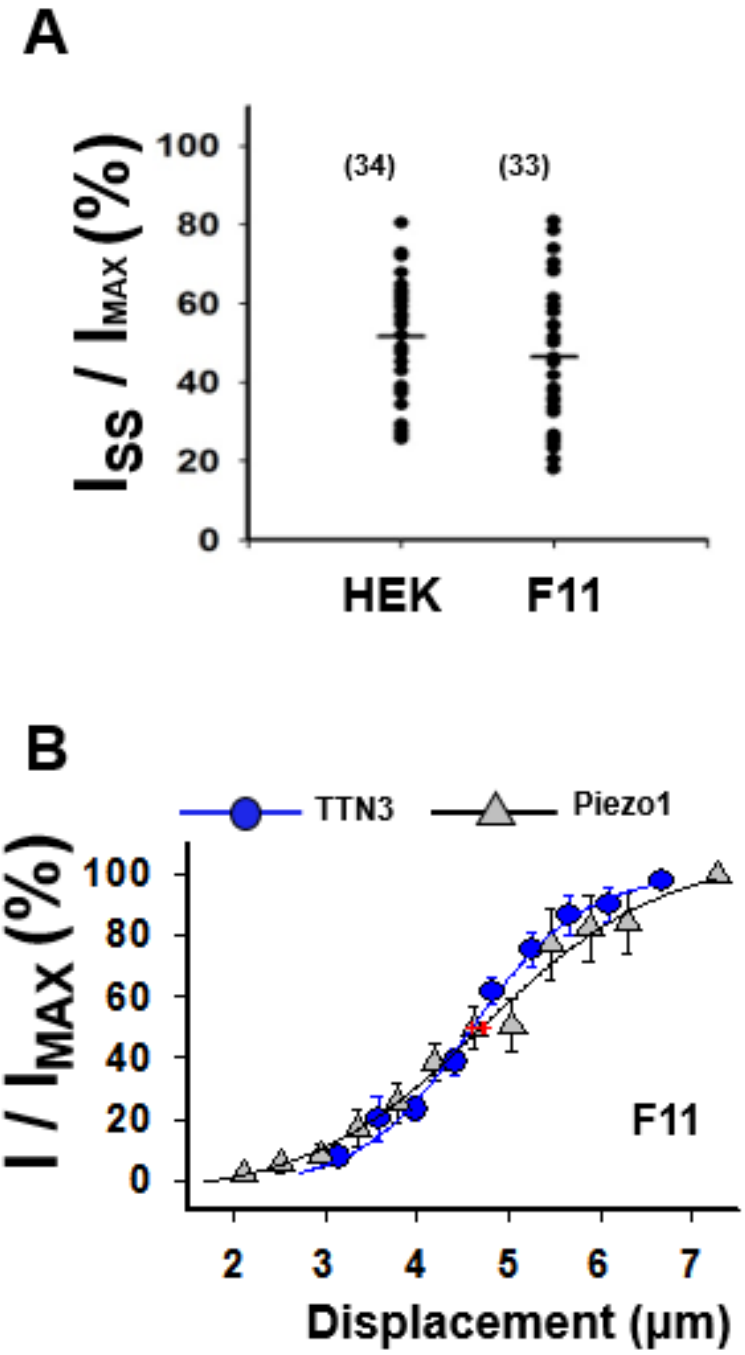
A
100
80
60
40
20
0
I_{SS} / I_{MAX} (%)
(34)
(33)
HEK
F11
B
TTN3
Piezo1
100
80
60
40
20
0
I / I_{MAX} (%)
F11
2
3
4
5
6
7
Displacement (µm)

Figure 14. Steady-state currents and displacement-response relationships of TTN3

A) Ratios between peak (I_{MAX}) and steady-state (I_{SS}) currents in *Ttn3*-transfected F11 and HEK293T cells. The steady-state currents were measured at 600 ms. A line represents the mean.

B) Displacement-response relationships of TTN3 and Piezo1 in F11 cells. MA currents (I) were normalized by maximal peak currents (I_{MAX}) activated by displacement of the mechanical stimulation. The mechanical steps were applied for 600 ms. Displacement represents the distance of the mechanical step from the surface of the cell. Normalized currents were fitted to a Boltzmann equation given by I/I_{MAX} (%) = $[(1+\exp(-(D-D_{1/2})/k))^{-1}]^{-1}$, where D is the indentation distance, $D_{1/2}$ is the half-maximal displacement and k is the response sensitivity to the indentation. Red dots represent the mean of $D_{1/2}$s.

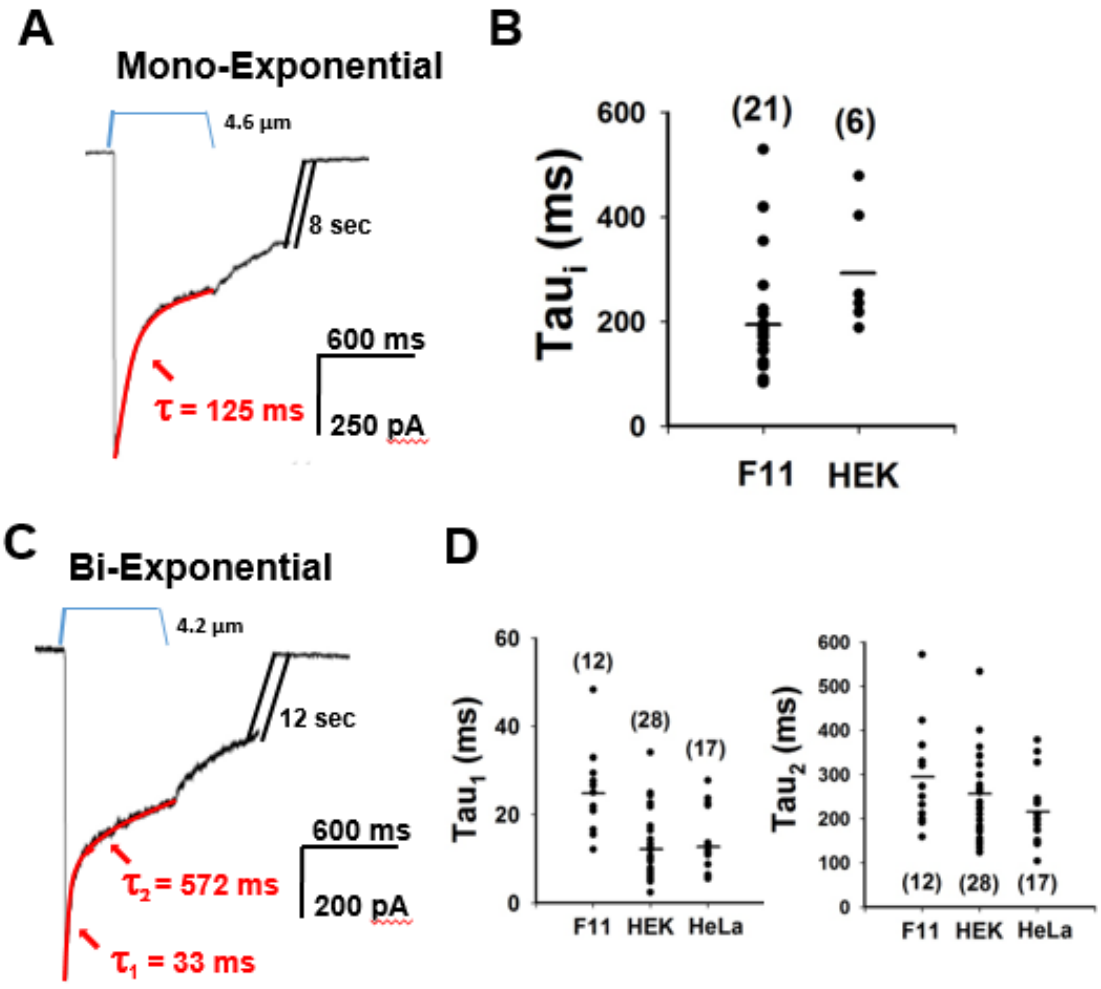
A
Mono-Exponential
4.6 µm
8 sec
600 ms
250 pA
τ = 125 ms
B
600
400
200
0
Tau$_i$ (ms)
(21)
(6)
F11
HEK
C
Bi-Exponential
4.2 µm
12 sec
600 ms
200 pA
τ$_2$ = 572 ms
τ$_1$ = 33 ms
D
60
40
20
0
Tau$_1$ (ms)
(12)
(28)
(17)
F11
HEK
HeLa
600
500
400
300
200
100
0
Tau$_2$ (ms)
(12)
(28)
(17)
F11
HEK
HeLa

Figure 15. The inactivation rates of TTN3 MA currents were fitted to mono- or bi-exponential curves

A) A representative trace of TTN3-MA currents in F11 cell whose inactivation rate was fitted to a mono-exponential curve.

B) Distribution of inactivation time constant Tau_i of TTN3 when expressed in HEK293T or F11 cells. Numbers in the bracket represent experimental numbers.

C) A representative trace of TTN3-MA currents in F11 cell whose inactivation rate was fitted to a bi-exponential curve.

D) Distribution of inactivation time constants Tau_1 and Tau_2 of TTN3 expressed in HEK293T, HeLa, and F11 cells. .

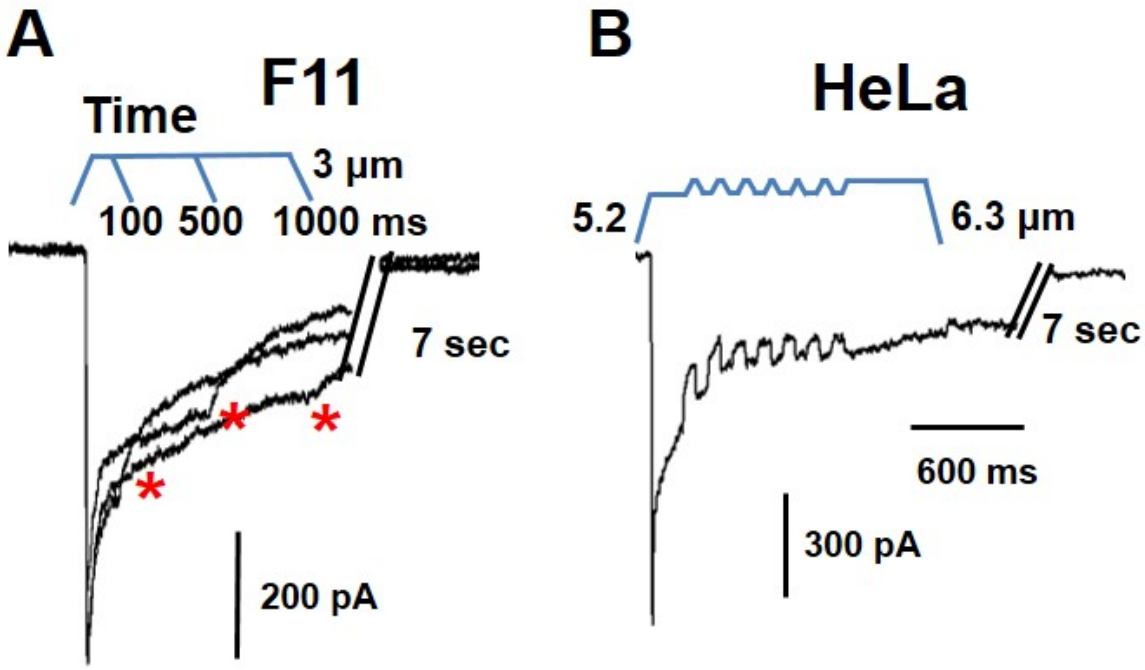

Figure 16. Biophysical properties of TTN3 MA current

A) The steady-state current of an *Ttn3*-transfected F11 cell persisted up to 1 s for a mechanical step. Asterisks represent steady-state currents at the end of the mechanical stimuli

B) A representative trace of sinusoidal steady-state currents that followed sinusoidal 1.1 µm mechanical steps after a 200 ms conditioning step. The MA currents were recorded in a HeLa cell transfected with *Ttn3*.

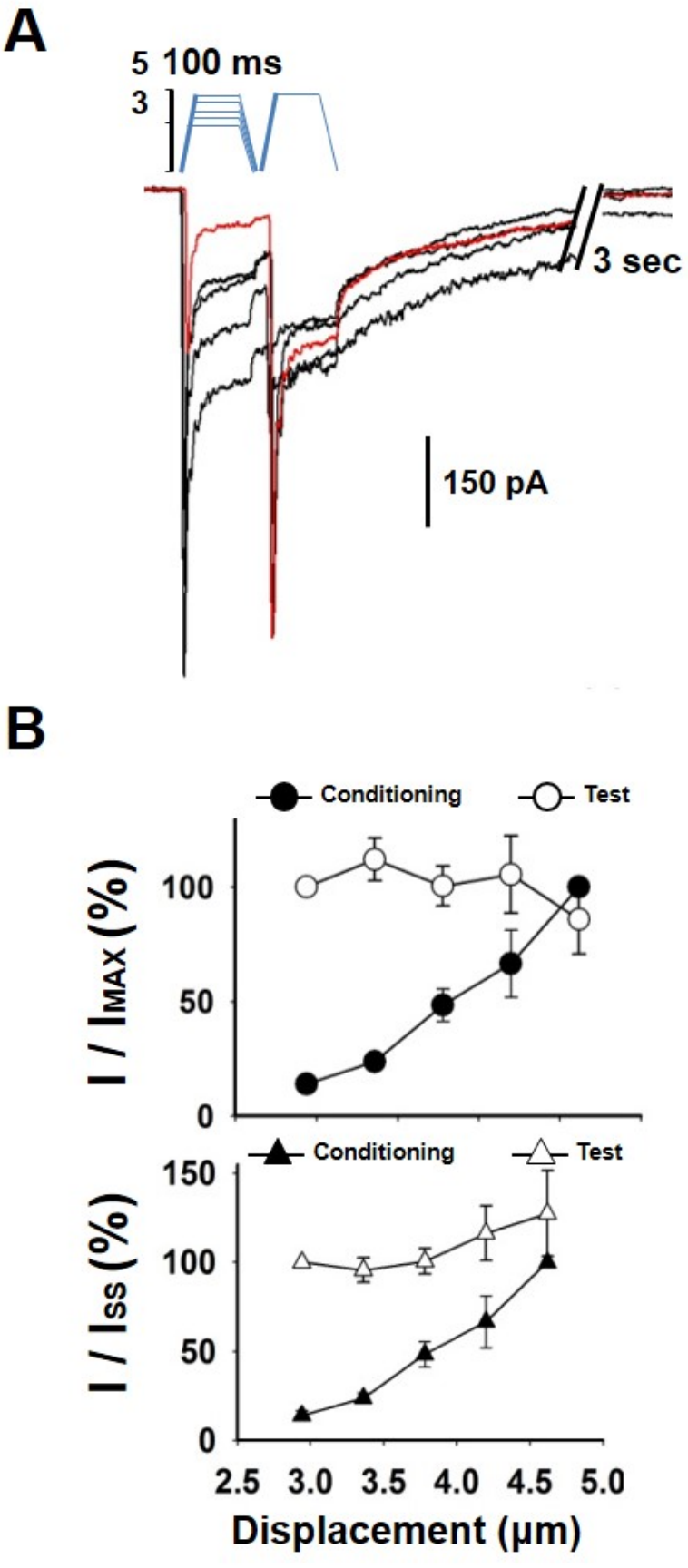
A
5
3
100 ms
3 sec
150 pA
B
Conditioning
Test
I / IMAX (%)
100
50
0
Conditioning
Test
I / Iss (%)
150
100
50
0
2.5
3.0
3.5
4.0
4.5
5.0
Displacement (μm)

Figure 17. Conditioning and test mechanical steps of TTN3 in F11 cells

A) The effects of conditioning stimuli on MA currents of *Ttn3*-transfected cells. Conditioning mechanical stimuli of 100 ms duration with 2.9–4.6 μm indentations with 0.42 μm increments were applied, followed by a test step pulse with a 4.6 μm stimulus.

B) Peak and steady-state currents induced by the conditioning and test mechanical steps. The peak or steady-state currents (I) were normalized with the maximal peak (I_{MAX}) or steady-state currents (I_{SS}). The steady-state currents were measured at the end of the mechanical steps (n = 4–5).

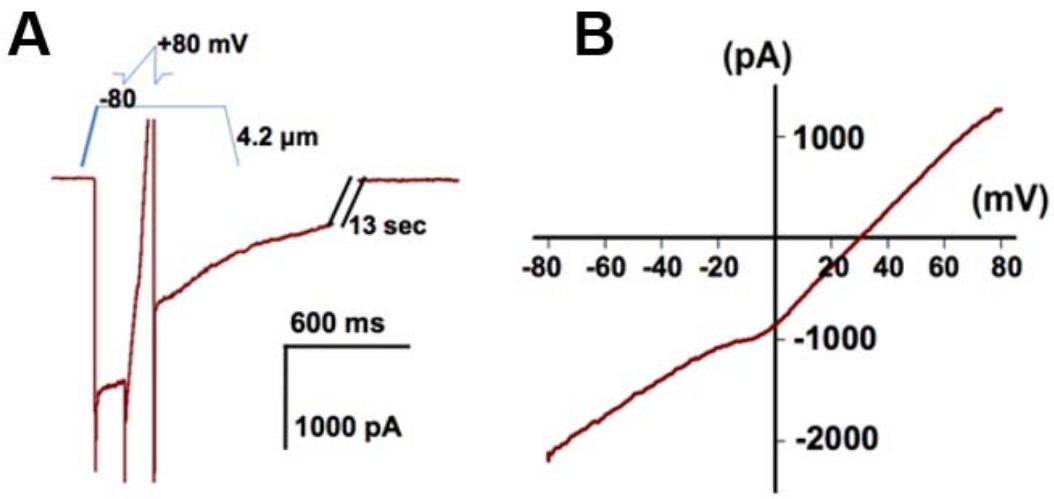

Figure 18. Measurement of TTN3 I-V relationship in F11 cells

A) A representative trace depicting current activated by a mechanical step and voltage ramp in an TTN3 expressing cell. The voltage-ramp from -80 to +80 mV was applied during the steady-state current. Ehold = -60 mV.

B) An I-V curve obtained with the voltage ramp.

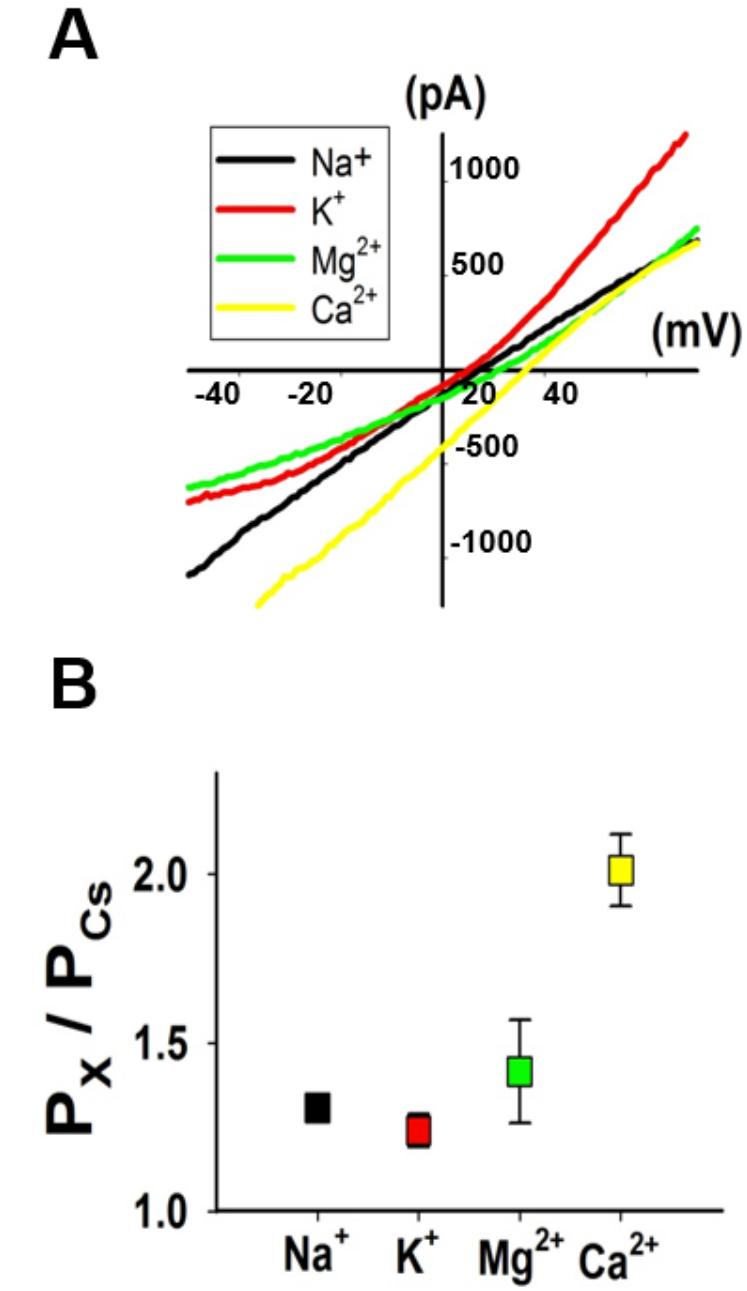
A
(pA)
Na+
K+
Mg2+
Ca2+
1000
500
(mV)
-40
-20
20
40
-500
-1000
B
PX / PCs
2.0
1.5
1.0
Na+
K+
Mg2+
Ca2+

Figure 19. Ion permeability of TTN3 determined by I-V relationships

A) Representative I-V relationships of steady-state MA currents obtained at different salt conditions in TTN3 overexpressing F11 cells. A voltage ramp (-80 to +80 mV) was applied within steady-state currents of TTN3 activation by mechanical stimuli. The pipette solution contained 150 mM CsCl. The bath solution contained 150 mM NaCl, 150 mM KCl, 100 mM $MgCl_2$, or 100 mM $CaCl_2$.

B) Cation permeability ratios (P_X/P_{Cs}) of the steady state MA currents in TTN3 expressing F11 cells (n = 6–9).

5. Putative pore region

To glean insights to the location of a pore, mutations were performed on a putative pore region. TTN3 has a pore-like reentry region between TM1 and TM2 (Fig. 20A). This region appears analogous to those in TM5 and TM6 reentry regions of transient receptor potential (TRP) as well as KcsA channels(Cao et al., 2013; Liao et al., 2013; Owsianik et al., 2006) . Recently, the structure of the selectivity filter of TRPV1 is revealed with cryo-electron microscope technique to resolution of ~4.0 angstrom (Cao et al., 2013; Liao et al., 2013). Cluster analysis of the region revealed that the amino-acid sequence of this region of mouse TTN3 was well aligned to the pore regions of TRPV channels. 48-**GAKH**-51 in TTN3 was aligned to the conserved **GMGD** residues in the selectivity filters of TRPV channels (Fig. 20A) (Cao et al., 2013; Liao et al., 2013; Owsianik et al., 2006). When Ala at 49 and His at 51 were changed to Lys and Asp, respectively, there were about three-fold increase in P_{Cl}/P_{Na} ratios (Fig. 20B), suggesting that the reentry region of TTN3 would be a putative pore region. Consequently, transition of ion conducting properties in TTN3-mediated current potently supports that TTN3 could be the major pore-forming unit of mechanically activating ion channel complex

A

```
TRPV1   -YNSLYSTCLELFKFTIGMDGLEFT
TRPV2   -YRGILEASLELFKFTIGMGELAFQ
TRPV4   -SETFSTFLLDLFKLTIGMGDLEML
hTTN3   -VEDDKILPLNSAERKPGVKHAPYI
mTTN3   -VEDDKILPLNSAARKSGAKHAPYI
```

B

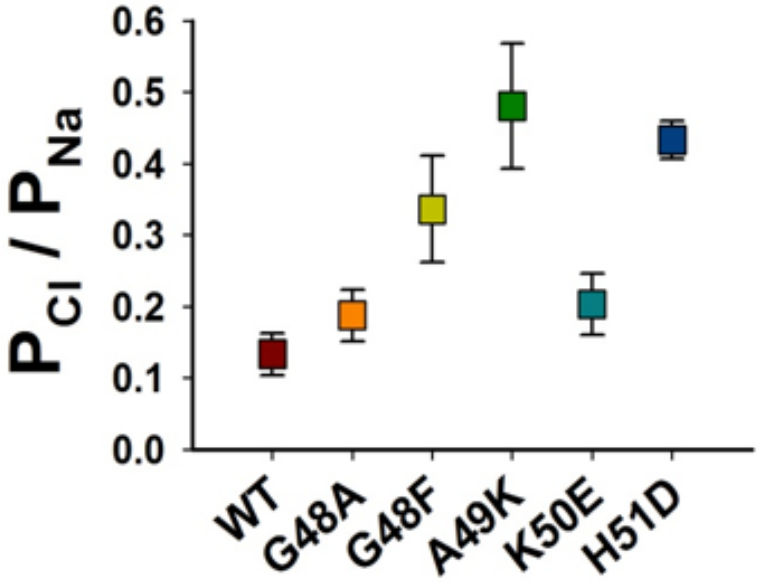

Figure 20. Changes in anion/cation permeability ratios (PCl/PNa) of wild-type (WT) and TTN3 mutants.

A) The alignment of amino-acid sequences of TRPV1, TRPV2, TRPV4, human TTN3 (hTTN3), and mouse TTN3 (mTTN3). Black bold letters represent the selectivity filters of TRPV channels.

B) Anion/cation permeability ratios (PCl/PNa) of wild-type (WT) and TTN3 mutants. WT or mutant TTN3 was transfected in F11 cells. The pipette and bath solutions contained 70 and 210 mM NaCl, respectively. The PCl/PNa of WT or each mutant was calculated by the reversal potential using the Goldman-Hodgkin-Katz equation (n = 7–9).

6. Pharmacology of TTN3

MA currents in DRG neurons are inhibited by gadolinium (Gd^{3+}) and other blockers (Drew et al., 2004; Drew and Wood, 2007; Drew et al., 2002a; McCarter et al., 1999b) . To determine the pharmacological profile of TTN3, F11 cells transfected with *Ttn3* were stimulated by three consecutive mechanical stimuli of identical amplitude (4.2 or 4.6 μm). The TTN3 MA currents were reversibly inhibited by known mechanosensitive channel blockers. The application of 30 μM Gd^{3+}, which is a well-known MA channel blocker (Coste et al., 2010; McCarter et al., 1999a), significantly inhibited the MA currents in TTN3-expressing cells (Fig. 4A). The half-maximal concentration for inhibition (IC_{50}) of Gd^{3+} was 3.9 μM (n = 7-8) (Fig. 22A). In addition, the TTN3 currents were markedly reduced by 30 μM ruthenium red or FM1-43, a fluorescent dye known to block MA currents in DRG neurons (Drew and Wood, 2007) (Fig. 21,22B). More importantly, 2.5 μM GsMTx4, a purified tarantula toxin that inhibits MA currents in various cell types, also strongly inhibited the TTN3 mediated MA currents (Bae et al., 2011; Gottlieb et al., 2007) (Fig. 21,21B). The TTN3 mediated MA currents were not blocked by 50 μM chloropromazine, a cup former membrane modifying agent that is known to inhibit the MA TREK1 channel (Maingret et al., 2000), or by 10 μM HC030031, a TRPA1 blocker known to inhibit mechanosensitive currents (Kerstein et al., 2009). Modification of the property in TTN3-mediated MA currents by these chemicals or

peptides also implies that TTN3 could be a major component of mechanosensitive ion channel.

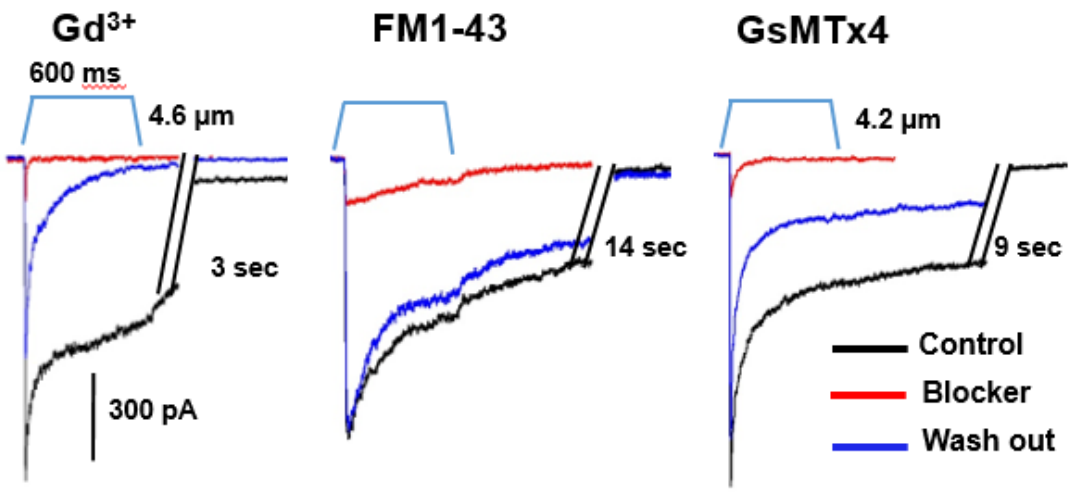

Figure 21. Inhibition of TTN3 MA currents by known MA channel blockers.

Representative traces of TTN3-mediated MA currents in F11 cells after the application of 30 µM gadolinium (Gd^{3+}), 30 µM FM1-43, or 2.5 µM GsMTx4. Identical mechanical steps were repeated three times. Each blocker was applied for 1 min before the second mechanical step, followed by wash out for recovery

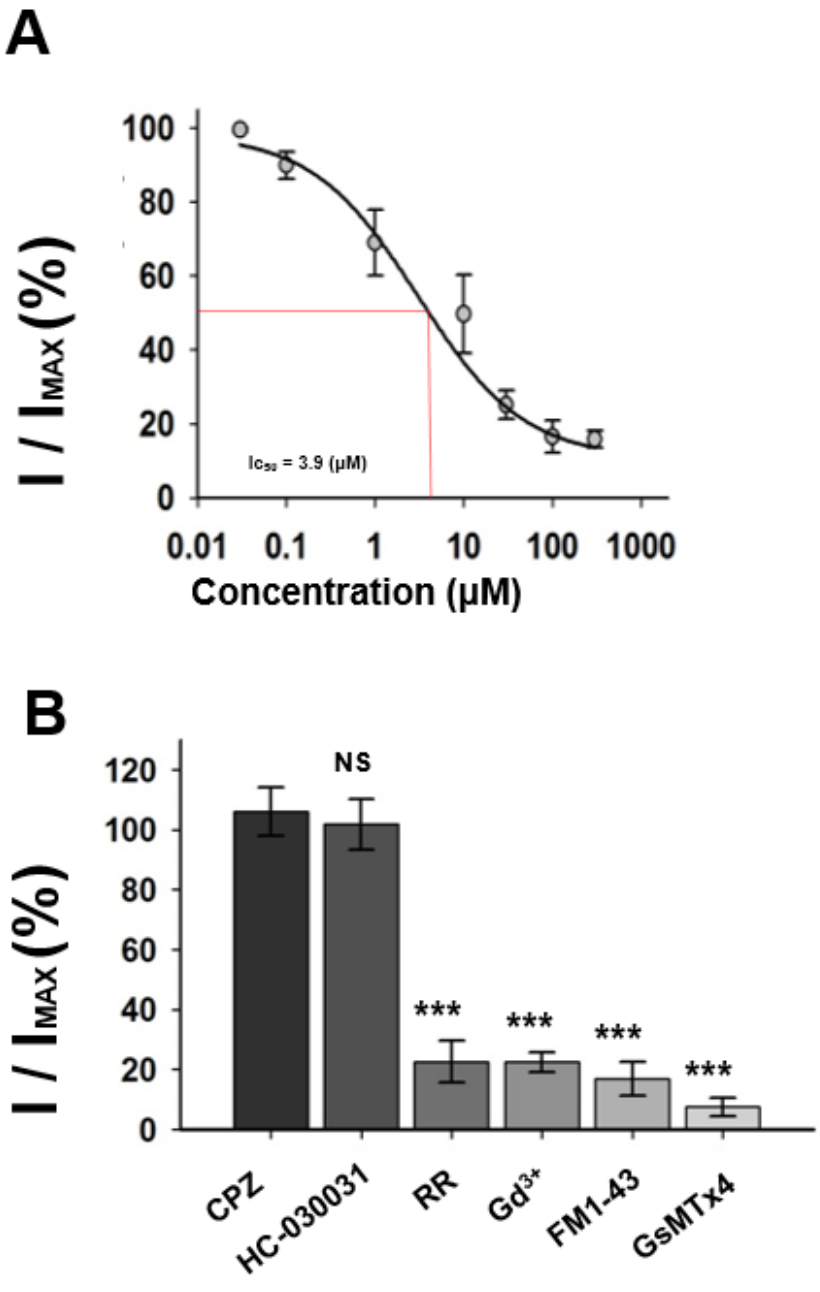
A
I / I MAX (%)
100
80
60
40
20
0
Ic50 = 3.9 (μM)
0.01
0.1
1
10
100
1000
Concentration (μM)
B
I / I MAX (%)
120
100
80
60
40
20
0
NS
***
***
***
***
CPZ
HC-030031
RR
Gd3+
FM1-43
GsMTx4

Figure 22. Pharmacological profiles of TTN3-mediated MA currents.

A) Dose-response relationship of Gd^{3+} in inhibiting the TTN3-mediated MA currents fitted to the Hill equation (IC_{50} = 3.9 μM, n = 7–8).

B) The effects of 50 μM chloropromazine (CPZ), 10 μM HC-030031, 30 μM ruthenium red (RR), 30 μM Gd^{3+}, 30 μM FM1-43, and 2.5 μM GsMTx4 on the TTN3-mediated MA currents (n = 7–8). ***$p < 0.001$ compared to the I/I_{MAX} of CPZ treatment, one-way ANOVA, Tukey's post-hoc test.

7. Expression of TTN3 in DRG neurons

A quantitative PCR assay of three *Ttn* genes from 21 mouse tissues depicted a different expression pattern for each gene (Fig. 23). TTN3 showed high expression in the epididymis, pancreas, DRG, eye, brain, and spinal cord. To observe the expression patterns of TTN3 in DRG, we generated anti-TTN3 antibody against a segment in the C-terminus. This antibody appears to be specific as it detected endogenous and overexpressed TTN3 but not in *Ttn3* siRNA transfected F11 cells (Fig. 24A). Furthermore, when TTN3-IRES2-AcGFP was transfected in HEK293T cells, the immunofluorescence of TTN3 was detected in GFP-expressing cells (Fig. 24B).

The immunofluorescence analysis of TTN3 in DRG neurons revealed unique expression pattern in DRG neuronal populations. About 61% (646/1,056 cells) of TTN3-positive cells were colocalized with neurofilament M, a marker for myelinated neurons (Fig. 25). In addition, 57% (499/878 cells) of TTN3-positive neurons were positive to parvalbumin, a marker for proprioceptive sensory neurons. TTN3-positive neurons were positive for nociceptor markers, TRPV1 (23%) or isolectin B4 (15%) (Fig. 25). We could not observe clear immunoreactivity in DRG neurons from *Ttn3* KO mice (Fig.26).

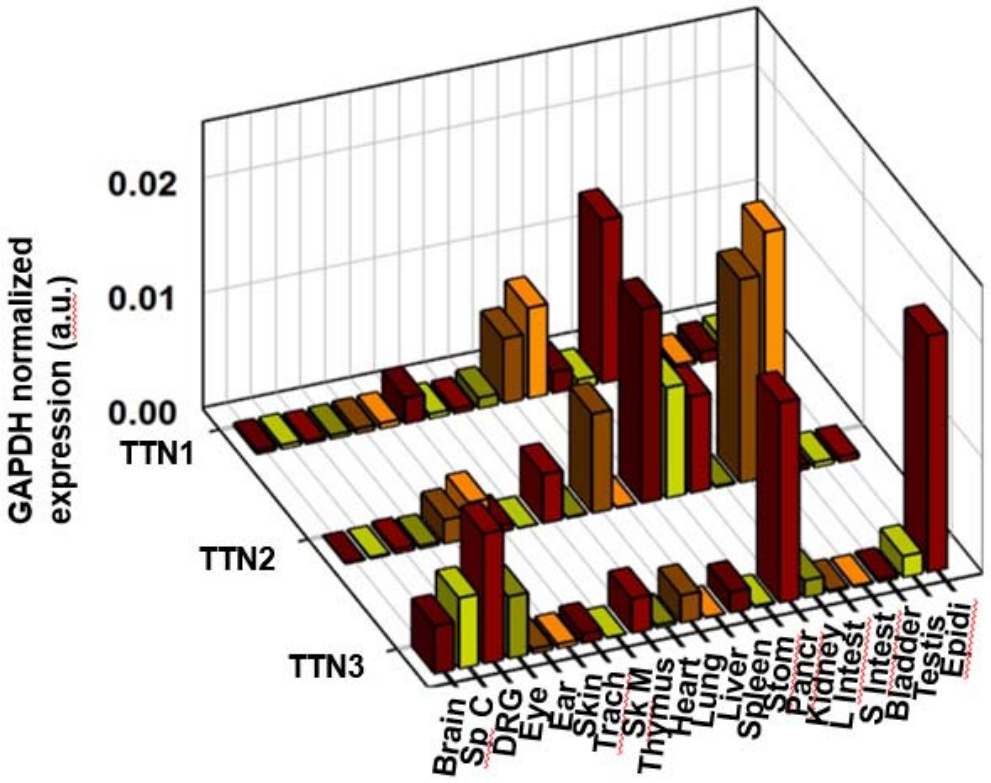

Figure 23. Expression profiles of *Ttn* genes.

Quantitative PCR was conducted from 21 adult mouse organs. The expression levels were normalized to the mRNA level of GAPDH. Bars represent the average of three experiments.

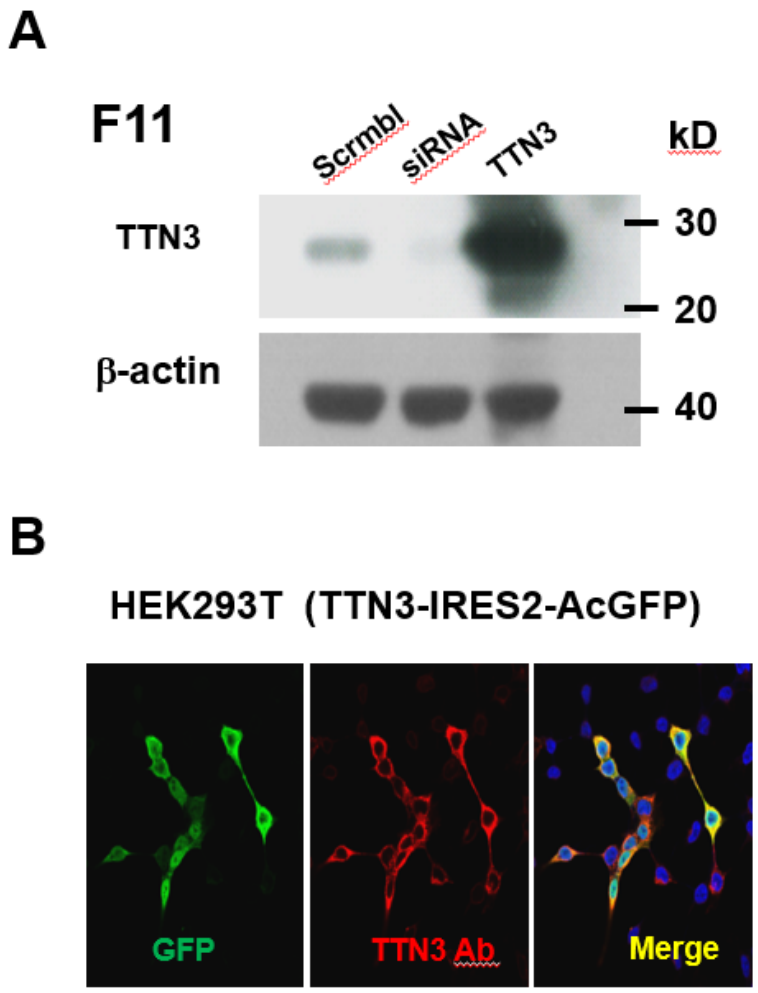

Figure 24. Validation of TTN3 antibody.

A) Western blots with anti-TTN3 antibody in F11 cells. F11 cells were transfected with scrambled siRNA (scrmbl), Ttn3 siRNA or TTN3-IRES2-AcGFP. β-actin was used as a control.

B) Immunofluorescent images in TTN3-IRES2-AcGFP transfected HEK293T cells stained with anti-TTN3 antibody.

A

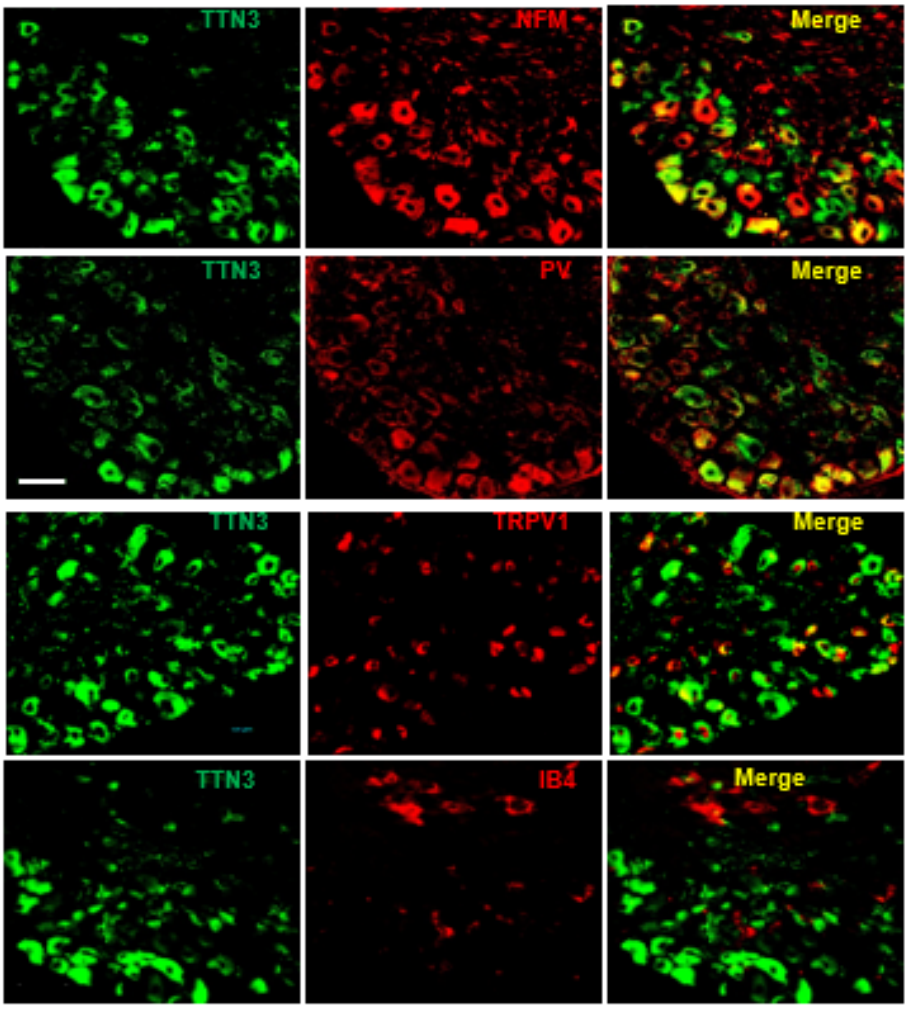
TTN3
NFM
Merge
TTN3
PV
Merge
TTN3
TRPV1
Merge
TTN3
IB4
Merge

B

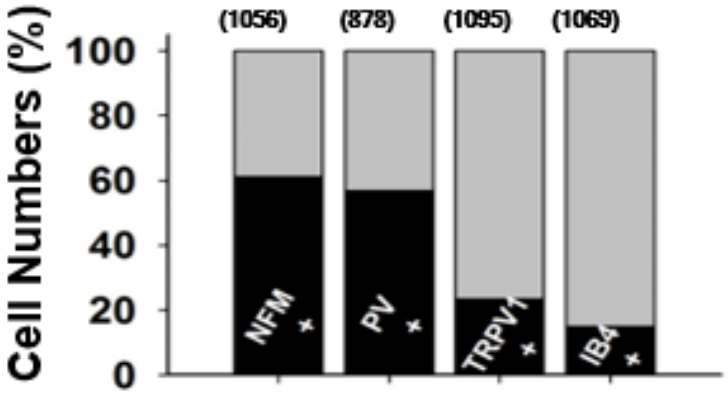
Cell Numbers (%)
100
80
60
40
20
0
(1056)
(878)
(1095)
(1069)
NFM
PV
TRPV1
IB4
*
*
*
*

Figure 25. Expression of TTN3 in mouse DRG neurons.

A) Representative immunofluorescent images of TTN3 with Neurofilament M (NFM), parvalbumin (PV), TRPV1 and Isolectin B4 (IB4).

B) The percentages of NFM, PV, TRPV1, and IB4-positive neurons in the TTN3-positive DRG neurons. The numbers in brackets represent the total number of TTN3-positive DRG neurons.

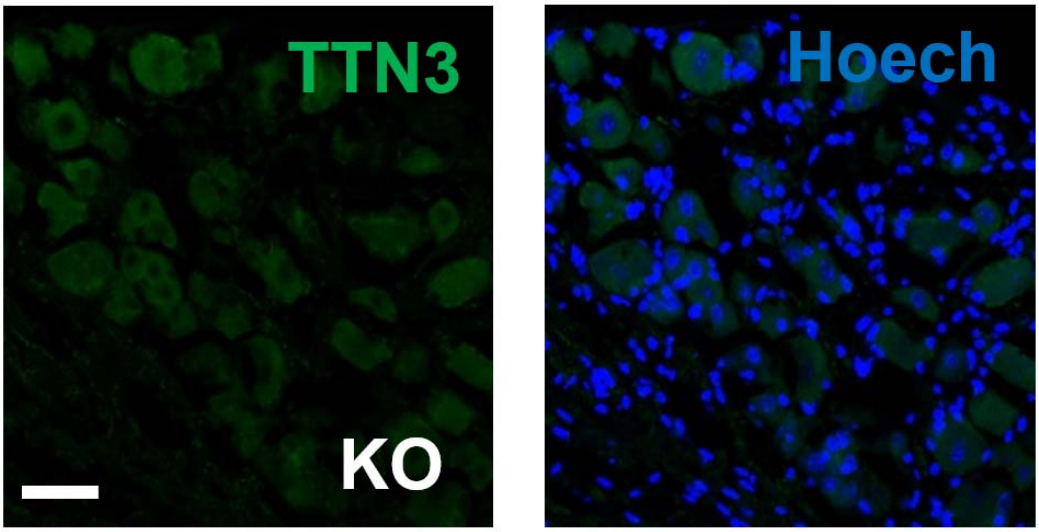

Figure 26. Expression of TTN3 in TTN3 KO DRG neurons.

Representative immunofluorescent images of TTN3 with Neurofilament M (NFM) in TTN3 KO DRG neurons.

8. Expression and functional role of TTN3 in muscle spindles

Rich immunoreactivity of TTN3 was observed in MSs in extensor digitorum longus (EDL) muscles of mouse hind limb (Fig. 27A). The TTN3 immunoreactivity was prominent in the center region of MSs where intrafusal muscle nuclei clustered (Barker, 1974; Bewick and Banks, 2015; Oliveira Fernandes and Tourtellotte, 2015; Tourtellotte and Milbrandt, 1998). In addition, TTN3 immunofluorescence was colocalized with neurofilament M in annulospiral structures wrapping round intrafusal muscles, typical primary afferents in MSs (Fig. 28A,B) (Banks, 2015; de Nooij et al., 2015; Oliveira Fernandes and Tourtellotte, 2015). However, the TTN3 immunofluorescence was not observed in MSs of *Ttn3*-KO mice (Fig. 28B).

The presence of TTN3 in MS prompted us to investigate the functional role of TTN3 in MS afferents by measuring MS afferent activities of wild-type (WT) and KO mice. Extracellular neural recording was made at the peroneal nerve attached to the isolated EDL muscle (de Nooij et al., 2015; Franco et al., 2014). Stretching the EDL muscles (~10 mm) isolated from WT mice by 2 mm for 5 sec evoked a barrage of nerve discharges. However, the activity of the muscle stretch-evoked discharge in MS afferents from KO mice was dramatically reduced (Fig. 29). The reduction in spindle afferent activity was observed throughout the range of muscle stretch (1–3 mm) ($p < 0.0001$, two-way ANOVA, $F_{(1,132)} = 56.5$). *Ttn3* KO mice showed a significant reduction

in the sensitivity (slope) to muscle stretch compare to WT mice (5.81 ± 0.72 vs 2.77 ± 0.36 spikes/mm, $p < 0.001$, n = 23–24, Student-t test) (Fig. 29B). These results indicate that TTN3 contributes to stretch-evoked MS afferent activity.

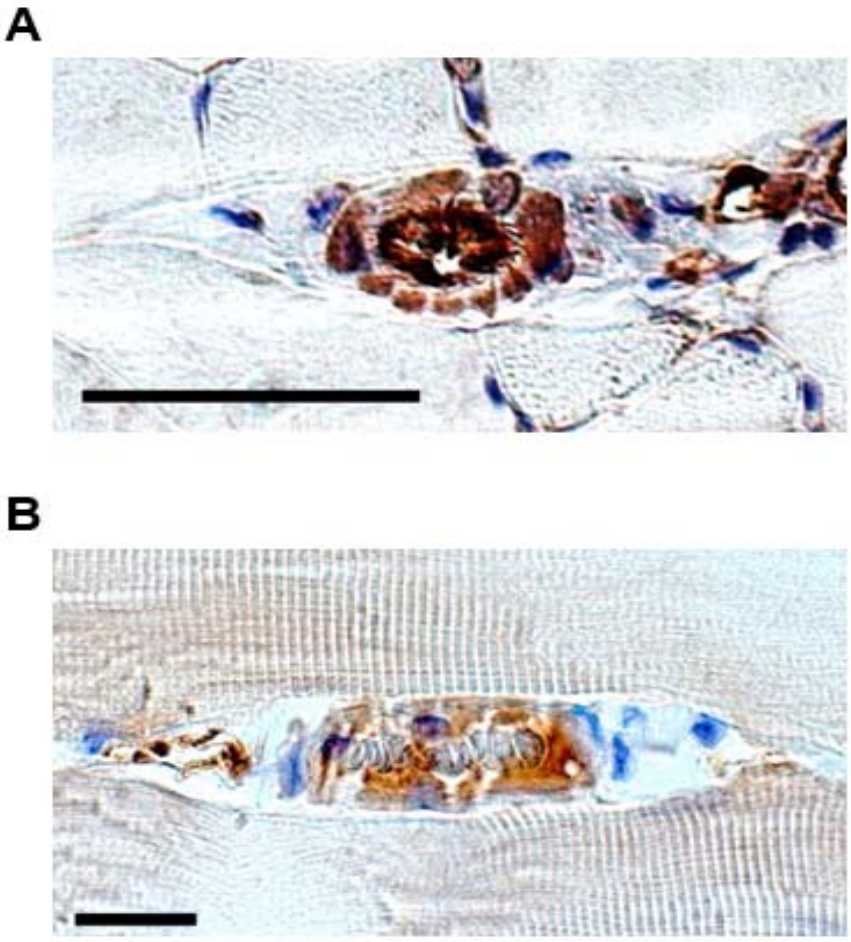

Figure 27. The presence of TTN3 in MSs determined by immunohistochemistry.

Immunohistochemistry of TTN3 in MSs of cross (A) and longitudinal (B) sections of EDL muscles. In cross section, heavy immunoreactivity of TTN3 was observed in intrafusal muscles. In longitudinal section, the TTN3 immunoreactivity surrounded nuclei of intrafusal muscles. H & E staining. Bars, 20 mm.

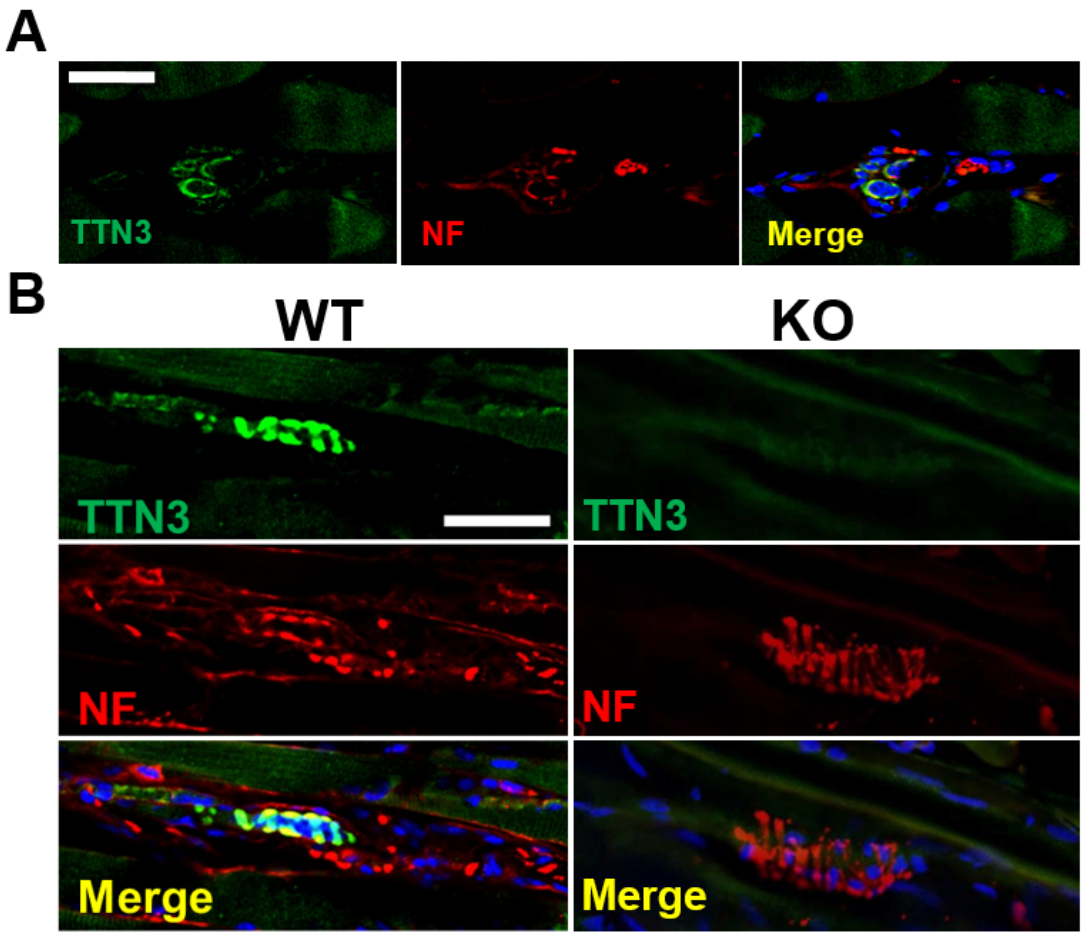

Figure 28. The presence of TTN3 in MSs determined by immunofluorescence.

TTN3 immunofluorescence surrounding intrafusal muscles and annulospiral fibers in MSs of cross (A) and longitudinal (B) sections of EDL muscles from wild-type (WT) and *Ttn3* KO mice. Part of TTN3 is colocalized with neurofilament (NF), a marker for myelinated nerve fibers. Nuclei were also stained in blue with Hoechst 33342.

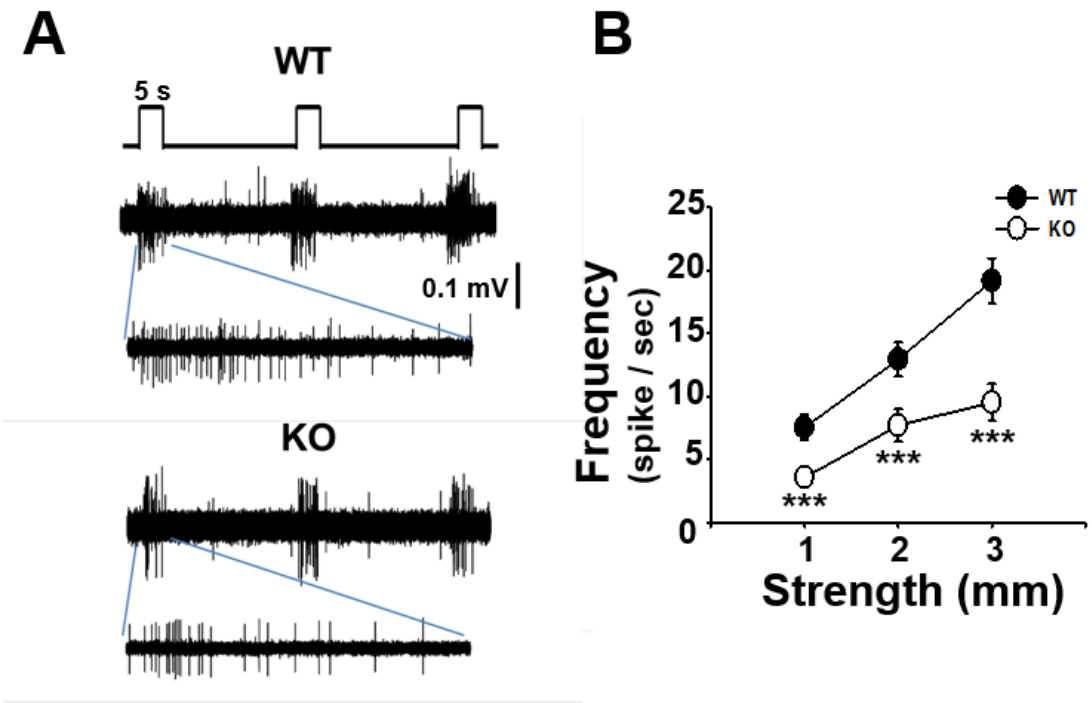

Figure 29. Reduction in stretch-evoked muscle afferent activity in *Ttn3* KO mice.

A) Stretch-evoked MS afferent activities of *ex-vivo* muscle-nerve preparation of WT and KO mice. MS afferent activities were recorded with a suction electrode (70 mm in diameter) from nerves attached to EDL muscles while muscles were stretched to 2 mm in length.

B) Summary of MS afferent activities of both genotypes in response to 1~3 mm stretches (n = 23–29). ***p < 0.001, Student's *t*-test.

9. Loss of motor coordination in Ttn3 KO mice

Because MS sensory input is essential for muscle coordination, behavior tests for determining muscle coordination were conducted. *Ttn3* KO mice spent less time clinging to an inverted grid compared to WT mice, a test for motor coordination and muscle strength because grip of the grid with all four limbs is required for prolonged hanging (Cheret et al., 2013). While WT mice continued to hang for longer than 10 minutes, the majority of KO mice fell within 2 minutes (Fig. 30A). In a raised beam test (Bourane et al., 2015; Muller et al., 2008), KO mice made about three times more limb-slips and showed significantly slower time to cross the beam (4.6 sec vs 6.5 sec, $p < 0.01$, $n = 10–11$, Student-t test) than that of WT mice (Fig. 30B). Furthermore, gait analysis with the CatWalk system revealed an abnormal gait in KO mice. The gait of KO mice showed significantly slower movement with reduced swing speed and stride length compared to WT mice (Fig. 31A-C). In addition, KO mice elicited reduced regularity index and phase dispersion in the fronto-hind limb coordination (Fig. 31D,E) (Dale et al., 2012; Encarnacion et al., 2011). In contrast, genetic ablation of *Ttn3* appeared not to affect general motor activity as well as tactile and pain sensation (Fig. 32,33). These results support the idea that TTN3 regulates motor coordination through MS afferents in mouse.

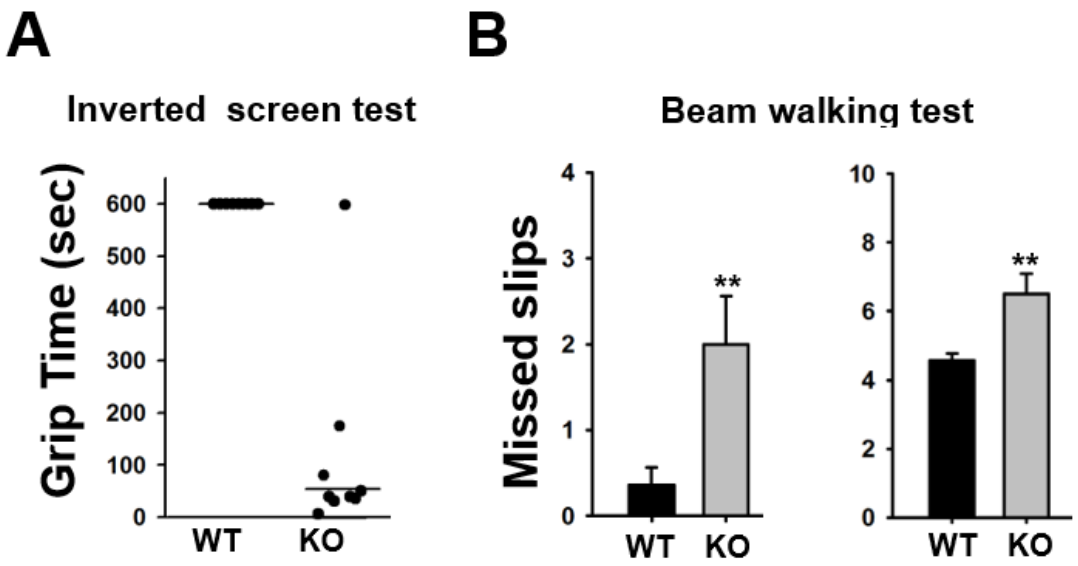

Figure 30. Loss of motor coordination in *Ttn3* KO mice.

A) Inverted screen test. Mice were hanged on an inverted grid screen. The duration of grip time of each mouse was measured. The cut-off time to cling to the inverted grid was 10 min. Horizontal bars represent average time to cling to the screen (n = 10–11). ***p < 0.001, Student's *t*-test.

B) Beam walking test. Mice were trained to walk on a 6 mm wide, 80-cm long beam. Their walk on the beam was video recorded and the number of missed slips and travelled time during walking were measured (n = 8–9). **p<0.01, Student's *t*-test.

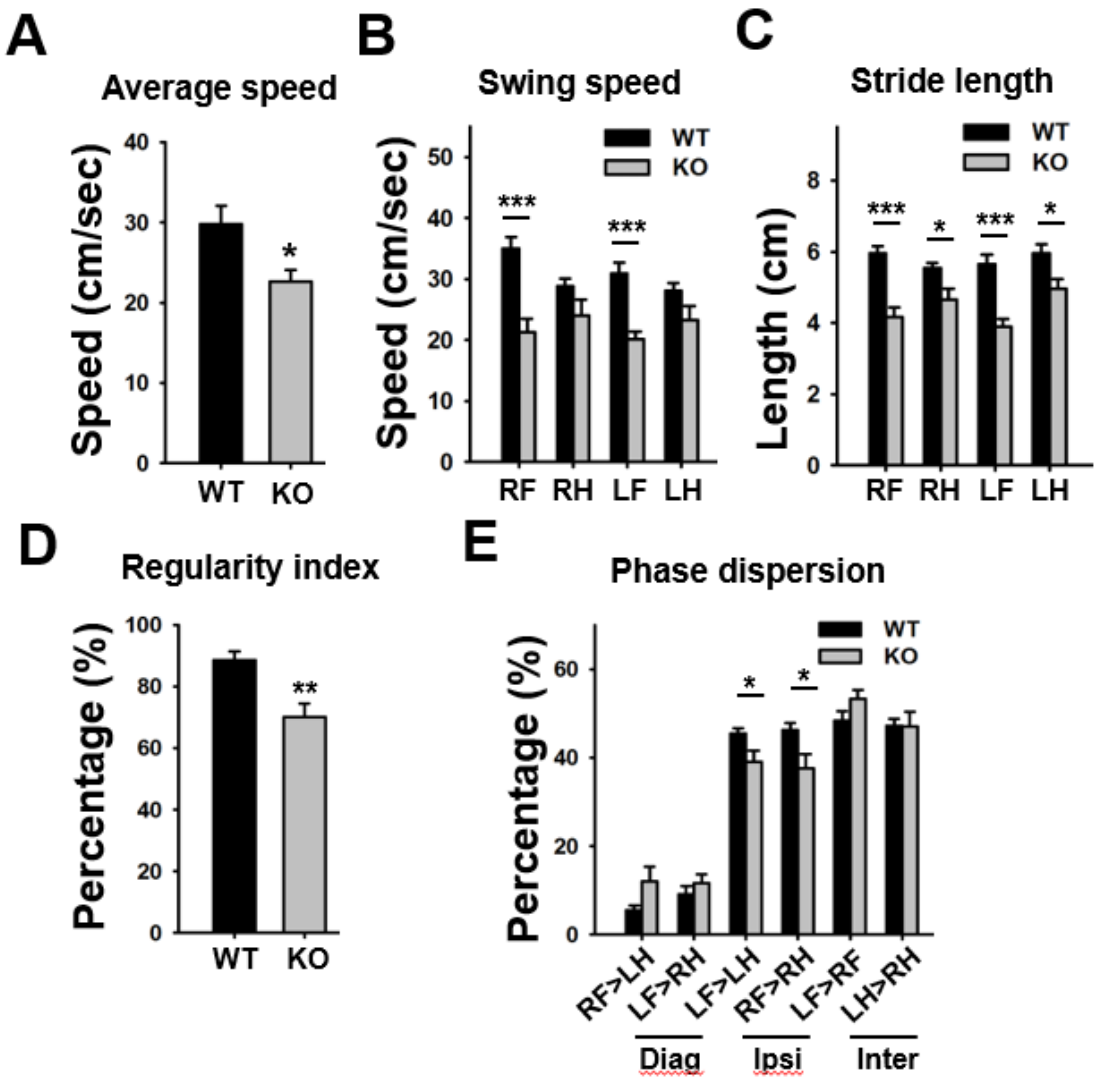
A
Average speed
Speed (cm/sec)
40
30
20
10
0
*
WT
KO
B
Swing speed
Speed (cm/sec)
50
40
30
20
10
0
WT
KO
***
***
RF
RH
LF
LH
C
Stride length
Length (cm)
8
6
4
2
0
WT
KO
***
*
***
*
RF
RH
LF
LH
D
Regularity index
Percentage (%)
100
80
60
40
20
0
**
WT
KO
E
Phase dispersion
Percentage (%)
60
40
20
0
WT
KO
*
*
RF>LH
LF>RH
LF>LH
RF>RH
LF>RF
LH>RH
Diag
Ipsi
Inter

Figure 31. Gait analysis of *Ttn3* KO mice with the Catwalk system.

Mice walked on a glass floor where their paw prints were recorded. KO mice showed slower walking (a) and swing (b) speed and shorter stride length (c) than those of WT mice. KO mice also showed lower regularity index (d) in their walking patterns and different phase dispersion (e) in fronto-hind limb coordination compared to WT mice. RF; right front paw, RH; right hind paw, LF; left front paw, LH; left hind paw, Diag; diagonal, Ipsi; ipsilateral, Inter; inter-limb (n= 8–10). *p<0.05, **p<0.01, ***p<0.001, Student's *t*-test.

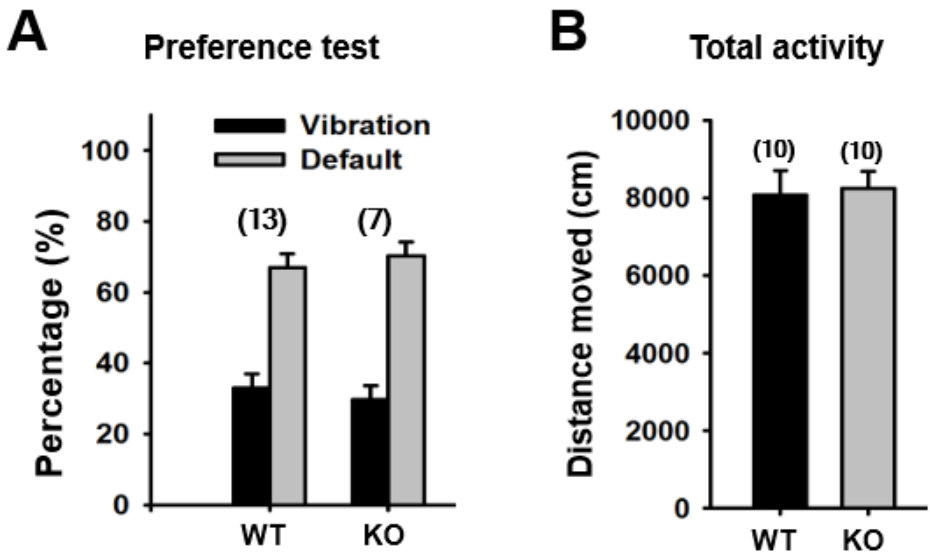

Figure 32. Behavioral tests for vibration preference and locomotor activity in Ttn3 KO mice.

A) Vibration preference test. Mice were placed in a chamber where two plates, one vibrating and non-vibrating plates were housed. Mice were allowed to wander around freely for 10 min. Time spent on each plate was measured from recorded video. The percentage of time represents the time spent on each plate divided by total time spent in the chamber.

B) Total distance of mice moved in an open field. The movement of a mouse was measured for 40 min.

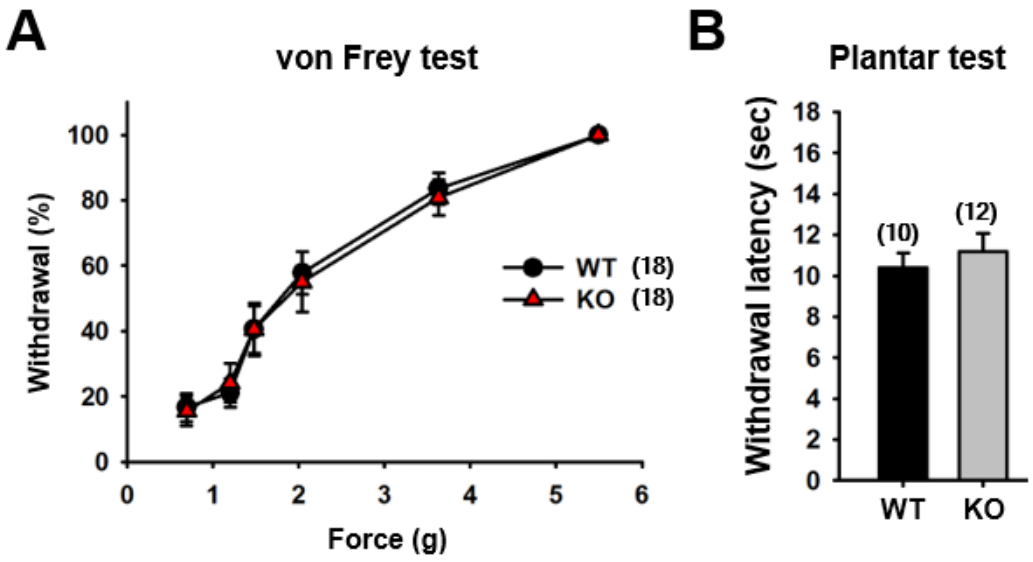

Figure 33. Behavioral tests for tactile and pain sensation in *Ttn3* KO mice

A) Withdrawal percentage of WT (●) and KO (▲) mice to von Frey hair stimuli. Both hind paws were stimulated with von Frey hairs. Withdrawal percentage was determined by the proportion of responses to four stimulations with each hair. (n = 9 each genotype).

B) Withdrawal latency of WT and KO mice to thermal stimuli in Hargreaves test. Radiant heat stimulus (IR = 50) was applied to left hind paws. Numbers in the bracket represent the number of experimental animals.

Discussion

Mechanosensation is essential for fundamental function of vertebrates including somatosensory sensation, proprioception, mastication, intestinal contraction, respiration, and blood pressure control. Moreover, tactile sensation is necessary for object recognition, movement, and social interactions with touch. The skin is the largest organ in our body equipped with specialized end organs or nerve terminals that detect tactile stimuli such as touch, pressure, or vibration. Among these tactile end organs in the skin are Merkel disk, Meissner's corpuscle, Ruffini ending and Pacinian corpuscles (Abraira and Ginty, 2013; Zimmerman et al., 2014). Recent advance in molecular imaging and optogenetics begins to uncover specific roles of these tactile mechanoreceptors in the skin (Zimmerman et al., 2014). However, the knowledge on the mechanoreceptors is still limited, largely because of the lack of molecular identity of MA channel genes.

Three types of MA currents, distinguished by their inactivation kinetics, are present in DRG neurons (Drew et al., 2004; Drew et al., 2002b; Hao and Delmas, 2010; Hu and Lewin, 2006). The kinetically defined MA DRG neurons fire differently in response to sustained tactile stimuli. The RA neurons tend to fire brief phasic

discharges, whereas the SA neurons elicit sustained discharges (Hao and Delmas, 2010). Piezo channels confer RA MA currents in many organs as well as DRG neurons. However, channel genes responsible for other kinetically defined currents in DRG neurons have not been identified. The present study provides evidence that TTN3 mediates SA currents in DRG neurons and presents typical biophysical and pharmacological profiles pertaining to SA mechanosensitive currents. Although there is a dramatic reduction in the number of SA-type neurons from *Ttn3*$^{-/-}$ mice, SA responses still remained in these mice. Thus, it is highly likely that there may be channels other than TTN3 that confer SA type currents.

In previous research, there are various types of pharmacological inhibitors of MS currents. FM1-43, a fluorescence dye for labelling membrane of cells is firstly discovered as a permeant blocker of inner and outer hair-cell MS channels in mouse cochlear. This agent vies with other cations for channel pore binding site and impedes influx of cations (Gale et al., 2001). Same in sensory neurons, three types of MS currents were found to be inhibited by FM1-43 and regulated by voltage and external Ca^{2+} concentration. FM1-43 also significantly modulated pain sensitivity determined by von Frey hair and Randall-Selitto test in mouse (Drew and Wood, 2007). Ruthenium red is previously known as a non-selective cation channel blocker such as transient receptor potential (TRP) channel family and it also inhibits MS currents in neurite and

human primary synovial fibroblasts (Jacques-Fricke et al., 2006; Sakamoto et al., 2010). Gadolinium is previously determined as blockers for cochlear hair cells in chick and several TRP channels including TRPV4 and TRPM3 (Holzer and Izzo, 2014; Kimitsuki et al., 1996). This ion blocks MS channel pore by competing with other cations. Most effective MS channel blocker is a tarantula spider toxin, GsMTx4 which is a 4kDa peptide. This toxin is thought to obstruct closed state of MS channels by changing local curvature of lipid bilayer and found to modulate a variety of mechanosensation related physiological processes (Gottlieb et al., 2007). Piezo-dependent RA current was profoundly inhibited by this peptide by micro molar concentrations (Bae et al., 2011).

In this study, we performed pharmacological profile of TTN3 using all known MS channel blockers. Indeed, Ruthenium red, FM1-43, Gadolinium and GsMTx4 dramatically inhibited TTN3 dependent MS current when expressed in F11 cell line. And several minutes after wash out these blockers, TTN3 current was almost recovered. However, other ion channel blockers such as chloropromazine and HC-030031 which are known to inhibit TREK and TRPA1 channels, respectively. Pharmacological property of TTN3 strengthens our notion that it is essential pore forming component of MS channel complex. In addition, we expect Pharmacological

study of TTN3 for future work will provide to medicalize motor dysfunction or other diseases related to mechanoperception.

Motor coordination is essential for survival, predation or escape. Without proper motor coordination, elaborate movements cannot be carried out because they require exact contraction timing of multiple flexor and extensor muscles. Motor coordination depends on proprioceptive sensory signals primarily from MS afferents in muscles (Proske and Gandevia, 2012; Proske et al., 2000; Rossi-Durand, 2006). Studies on genetic disruption of MS afferents supports the requirement of MS afferents for motor coordination (Cheret et al., 2013; Oliveira Fernandes and Tourtellotte, 2015; Tourtellotte and Milbrandt, 1998). During active muscle contraction or passive movements, MSs sense muscle stretch and report changes in length to the central nervous system (Banks, 1994; Ellaway et al., 2015). In the present study, TTN3 was expressed in MSs and the genetic ablation of TTN3 lead to a reduction in motor coordination. Thus, TTN3 appears to play a role in proprioception.

A skeletal muscle contains multiple MSs. The number of MSs varies in different muscles. In general, the density is high in muscles conducting fine movements such as interrossei muscles in hand whereas its density is low in girdle muscles (Barker, 1974). MSs are found only in vertebrates in the animal kingdom (Barker, 1974). The structure of MS varies among vertebrates such that primitive forms of MSs were found

in Amphibia (Barker, 1974). The presence of MSs in fish was controversial. Barker (1974) claimed that the fish does not have MSs (Barker, 1974). However, Maeda and colleagues found MSs in a jaw closing muscle in a Japanese salmon (Maeda et al., 1983). Consistent with this, *Ttn* genes were found in all vertebrates including chicken, turtle, frog, and zebrafish (Fig. 9).

The study of the ionic basis for receptor potential of MS afferents revealed that Na^+ and Ca^{2+} are responsible for the stretch-evoked receptor potential (Hunt et al., 1978). Thus, cationic channels were considered to be candidate channels for the mechanotransduction in MSs. Among them, epithelium sodium channel (ENaC) was considered to be a candidate (Bewick and Banks, 2015). ENaC is a mammalian homolog of DEG channel found in C. elegance. ENaC is highly selective to Na^+ and blocked by amiloride (Garty and Palmer, 1997). ENaC immunoreactivity is found in MS afferents (Simon et al., 2010). Moreover, the activity of MS afferent is largely inhibited by the amiloride application (Simon et al., 2010). These results suggest that ENaC appears to be a mechanotransduction channel in MS afferents. However, the mechanosensitivity of ENaC channel in mammals was controversial, because it is not activated by mechanical stimuli when expressed heterologously in mammalian cells (Awayda and Subramanyam, 1998; Drew et al., 2004). In addition, the loss-of-function phenotype for motor coordination has not been reported with ENaC-deficient mice.

Recently, Piezo2 is implicated in proprioception (Woo et al., 2015b). Woo and colleagues found that Piezo2 is present in MSs and its genetic deletion from muscle afferents leads to marked reduction in stretch-induced nerve activity of MS afferents as well as prominent loss of muscle coordination (Woo et al., 2015b). Thus, Piezo2 is a major stretch-activated channel responsible for the ionic basis of MS afferents. Although the prominent phenotype of Piezo2-deficient mice undoubtedly stresses its roles in proprioception, this does not preclude the possible presence of other MA channels for proprioception. The inactivation kinetic of Piezo2 does not fit in the kinetics of MS afferent responses. Piezo2 inactivates rapidly after a brief activation, whereas most MS afferents respond as long as muscle stretch lasts. In addition, there would be a redundancy of genes in proprioception, which is also the case in other key physiological functions such as heat sensation in the skin (Bandell and Patapoutian, 2012; Dhaka et al., 2006).

The function of the TMEM150/Tentonin genes is largely unknown except for a genetic link between TMEM150B/BRSK1 and menopause in women (He et al., 2009). Because of the low sequence similarity of TTN1 or TTN2 to TTN3, the function of TTN3 is unknown. Among these *Ttn* genes, only *Ttn3* responded well to mechanical stimuli. Although TTN3 can generate MA currents when expressed heterologously, the propensity of channel currents after transfection differs in cell types. Thus, whether it

is activated by a direct stretch of the plasma membrane or with the help of tethering proteins remains to be clarified.

MEC-2 is an associated protein with MEC-4 and MEC-10, degenerin genes encoding MA currents in touch receptors of *C. elegans* (Huang et al., 1995). *C. elegans* carrying *mec-2* null alleles lose touch sensitive behaviors. MEC-2 contains stomatin domain in its central region and belongs to stomatin-like proteins (Lapatsina et al., 2012). SLP3 is a mammalian homolog of MEC-2 because of its 77% similarity in amino-acid sequence with MEC-2 and its expression in DRG neurons (Wetzel et al., 2007). More importantly, *Slp3*$^{-/-}$ mice elicited a reduction in the proportion of SA MA currents in DRG neurons along with the reduction in tactile discrimination and mechanical allodynia, suggesting its functional association with mechanical transducer channels (Wetzel et al., 2007). SLP3 associates with Piezo2 and tunes its activity (Poole et al., 2014). SLP3 co-expression with Piezo2 largely augments the amplitude of MA piezo2 currents and lowers the threshold for the mechanosensitivity (Poole et al., 2014). In addition, SLP3 inhibits the acid-induced activity of ASIC channels in DRG neurons (Brand et al., 2012; Kozlenkov et al., 2014; Wetzel et al., 2007). Similarly, SLP3 may also control the TTN3 activity and further study of TTN3 with SLP3 will uncover functional association of each other.

Because MS afferent function is essential for motor coordination, the identification of the mechanotransduction channel in MS afferents provides a route to dissecting out the molecular mechanisms underlying motor coordination, which may be significant for understanding motor dysfunction in various human diseases. Identification of novel mechanosensitive ion channel will provide deeper understanding of uncovered various mechanosensations in mammals.

References

Abboud, F.M., and Benson, C.J. (2015). ASICs and cardiovascular homeostasis. Neuropharmacology *94*, 87-98.

Abraira, V.E., and Ginty, D.D. (2013). The sensory neurons of touch. Neuron *79*, 618-639.

Ahmed, Z.M., Goodyear, R., Riazuddin, S., Lagziel, A., Legan, P.K., Behra, M., Burgess, S.M., Lilley, K.S., Wilcox, E.R., Riazuddin, S.*, et al.* (2006). The tip-link antigen, a protein associated with the transduction complex of sensory hair cells, is protocadherin-15. J Neurosci *26*, 7022-7034.

Arnadottir, J., and Chalfie, M. (2010). Eukaryotic mechanosensitive channels. Annu Rev Biophys *39*, 111-137.

Arreola, J., and Melvin, J.E. (2003). A novel chloride conductance activated by extracellular ATP in mouse parotid acinar cells. J Physiol *547*, 197-208.

Awayda, M.S., and Subramanyam, M. (1998). Regulation of the epithelial Na+ channel by membrane tension. J Gen Physiol *112*, 97-111.

Bae, C., Sachs, F., and Gottlieb, P.A. (2011). The mechanosensitive ion channel Piezo1 is inhibited by the peptide GsMTx4. Biochemistry *50*, 6295-6300.

Bandell, M., and Patapoutian, A. (2012). A hot new channel. Nat Neurosci *15*, 931-933.

Banks, R.W. (1994). The motor innervation of mammalian muscle spindles. Progress in neurobiology *43*, 323-362.

Banks, R.W. (2015). The innervation of the muscle spindle: a personal history. J Anat *227*, 115-135.

Barker, D. (1974). The Morphology of Muscle Receptors. In Muscle Receptors, C.C. Hunt, ed. (New York: Springer-Verlag), pp. 1-190.

Bewick, G.S., and Banks, R.W. (2015). Mechanotransduction in the muscle spindle. Pflugers Arch *467*, 175-190.

Bourane, S., Grossmann, K.S., Britz, O., Dalet, A., Del Barrio, M.G., Stam, F.J., Garcia-Campmany, L., Koch, S., and Goulding, M. (2015). Identification of a spinal circuit for light touch and fine motor control. Cell *160*, 503-515.

Brand, J., Smith, E.S., Schwefel, D., Lapatsina, L., Poole, K., Omerbasic, D., Kozlenkov, A., Behlke, J., Lewin, G.R., and Daumke, O. (2012). A stomatin dimer modulates the activity of acid-sensing ion channels. Embo J *31*, 3635-3646.

Cao, E., Liao, M., Cheng, Y., and Julius, D. (2013). TRPV1 structures in distinct conformations reveal activation mechanisms. Nature *504*, 113-118.

Carter, R.J., Morton, J., and Dunnett, S.B. (2001). Motor coordination and balance in

rodents. Curr Protoc Neurosci *Chapter 8*, Unit 8 12.

Cassani, J., Ferreyra-Cruz, O.A., Dorantes-Barron, A.M., Villasenor, R.M., Arrieta-Baez, D., and Estrada-Reyes, R. (2015). Antidepressant-like and toxicological effects of a standardized aqueous extract of Chrysactinia mexicana A. Gray (Asteraceae) in mice. J Ethnopharmacol *171*, 295-306.

Cheret, C., Willem, M., Fricker, F.R., Wende, H., Wulf-Goldenberg, A., Tahirovic, S., Nave, K.A., Saftig, P., Haass, C., Garratt, A.N.*, et al.* (2013). Bace1 and Neuregulin-1 cooperate to control formation and maintenance of muscle spindles. Embo J *32*, 2015-2028.

Cho, H., Yang, Y.D., Lee, J., Lee, B., Kim, T., Jang, Y., Back, S.K., Na, H.S., Harfe, B.D., Wang, F.*, et al.* (2012). The calcium-activated chloride channel anoctamin 1 acts as a heat sensor in nociceptive neurons. Nat Neurosci *15*, 1015-1021.

Chort, A., Alves, S., Marinello, M., Dufresnois, B., Dornbierer, J.G., Tesson, C., Latouche, M., Baker, D.P., Barkats, M., El Hachimi, K.H.*, et al.* (2013). Interferon beta induces clearance of mutant ataxin 7 and improves locomotion in SCA7 knock-in mice. Brain *136*, 1732-1745.

Coste, B., Mathur, J., Schmidt, M., Earley, T.J., Ranade, S., Petrus, M.J., Dubin, A.E., and Patapoutian, A. (2010). Piezo1 and Piezo2 are essential components of distinct mechanically activated cation channels. Science *330*, 55-60.

Cote, M.P., Detloff, M.R., Wade, R.E., Jr., Lemay, M.A., and Houle, J.D. (2012). Plasticity in ascending long propriospinal and descending supraspinal pathways in chronic cervical spinal cord injured rats. Front Physiol *3*, 330.

Dale, J.M., Villalon, E., Shannon, S.G., Barry, D.M., Markey, R.M., Garcia, V.B., and Garcia, M.L. (2012). Expressing hNF-LE397K results in abnormal gaiting in a transgenic model of CMT2E. Genes Brain Behav *11*, 360-365.

de Nooij, J.C., Simon, C.M., Simon, A., Doobar, S., Steel, K.P., Banks, R.W., Mentis, G.Z., Bewick, G.S., and Jessell, T.M. (2015). The PDZ-domain protein Whirlin facilitates mechanosensory signaling in mammalian proprioceptors. J Neurosci *35*, 3073-3084.

Delmas, P., and Coste, B. (2013). Mechano-gated ion channels in sensory systems. Cell *155*, 278-284.

Delmas, P., Hao, J., and Rodat-Despoix, L. (2011). Molecular mechanisms of mechanotransduction in mammalian sensory neurons. Nat Rev Neurosci *12*, 139-153.

Dhaka, A., Viswanath, V., and Patapoutian, A. (2006). Trp ion channels and temperature sensation. Annu Rev Neurosci *29*, 135-161.

Drew, L.J., Rohrer, D.K., Price, M.P., Blaver, K.E., Cockayne, D.A., Cesare, P., and Wood, J.N. (2004). Acid-sensing ion channels ASIC2 and ASIC3 do not contribute

to mechanically activated currents in mammalian sensory neurones. J Physiol *556*, 691-710.

Drew, L.J., and Wood, J.N. (2007). FM1-43 is a permeant blocker of mechanosensitive ion channels in sensory neurons and inhibits behavioural responses to mechanical stimuli. Mol Pain *3*, 1.

Drew, L.J., Wood, J.N., and Cesare, P. (2002). Distinct mechanosensitive properties of capsaicin-sensitive and -insensitive sensory neurons. J Neurosci *22*, RC228.

Ellaway, P.H., Taylor, A., and Durbaba, R. (2015). Muscle spindle and fusimotor activity in locomotion. J Anat *227*, 157-166.

Encarnacion, A., Horie, N., Keren-Gill, H., Bliss, T.M., Steinberg, G.K., and Shamloo, M. (2011). Long-term behavioral assessment of function in an experimental model for ischemic stroke. J Neurosci Methods *196*, 247-257.

Franco, J.A., Kloefkorn, H.E., Hochman, S., and Wilkinson, K.A. (2014). An in vitro adult mouse muscle-nerve preparation for studying the firing properties of muscle afferents. J Vis Exp, 51948.

Gale, J.E., Marcotti, W., Kennedy, H.J., Kros, C.J., and Richardson, G.P. (2001). FM1-43 dye behaves as a permeant blocker of the hair-cell mechanotransducer channel. J Neurosci *21*, 7013-7025.

Garty, H., and Palmer, L.G. (1997). Epithelial sodium channels: function, structure,

and regulation. Physiol Rev *77*, 359-396.

Ghil, S.H., Kim, B.J., Lee, Y.D., and Suh-Kim, H. (2000). Neurite outgrowth induced by cyclic AMP can be modulated by the alpha subunit of Go. J Neurochem *74*, 151-158.

Gottlieb, P.A., Suchyna, T.M., and Sachs, F. (2007). Properties and Mechanism of the Mechanosensitive Ion Channel Inhibitor GsMTx4, a Therapeutic Peptide Derived from Tarantula Venom. Curr Top Membr *59*, 81-109.

Hamers, F.P., Koopmans, G.C., and Joosten, E.A. (2006). CatWalk-assisted gait analysis in the assessment of spinal cord injury. J Neurotrauma *23*, 537-548.

Hao, J., and Delmas, P. (2010). Multiple desensitization mechanisms of mechanotransducer channels shape firing of mechanosensory neurons. J Neurosci *30*, 13384-13395.

He, C., Kraft, P., Chen, C., Buring, J.E., Pare, G., Hankinson, S.E., Chanock, S.J., Ridker, P.M., Hunter, D.J., and Chasman, D.I. (2009). Genome-wide association studies identify loci associated with age at menarche and age at natural menopause. Nat Genet *41*, 724-728.

Holt, J.R., Pan, B., Koussa, M.A., and Asai, Y. (2014). TMC function in hair cell transduction. Hear Res *311*, 17-24.

Holzer, P., and Izzo, A.A. (2014). The pharmacology of TRP channels. Br J Pharmacol

171, 2469-2473.

Hu, J., and Lewin, G.R. (2006). Mechanosensitive currents in the neurites of cultured mouse sensory neurones. J Physiol *577*, 815-828.

Huang, M., Gu, G., Ferguson, E.L., and Chalfie, M. (1995). A stomatin-like protein necessary for mechanosensation in C. elegans. Nature *378*, 292-295.

Hunt, C.C., Wilkinson, R.S., and Fukami, Y. (1978). Ionic basis of the receptor potential in primary endings of mammalian muscle spindles. J Gen Physiol *71*, 683-698.

Jacques-Fricke, B.T., Seow, Y., Gottlieb, P.A., Sachs, F., and Gomez, T.M. (2006). Ca2+ influx through mechanosensitive channels inhibits neurite outgrowth in opposition to other influx pathways and release from intracellular stores. J Neurosci *26*, 5656-5664.

Jeyakumar, M., Butters, T.D., Cortina-Borja, M., Hunnam, V., Proia, R.L., Perry, V.H., Dwek, R.A., and Platt, F.M. (1999). Delayed symptom onset and increased life expectancy in Sandhoff disease mice treated with N-butyldeoxynojirimycin. Proc Natl Acad Sci U S A *96*, 6388-6393.

Kawashima, Y., Geleoc, G.S., Kurima, K., Labay, V., Lelli, A., Asai, Y., Makishima, T., Wu, D.K., Della Santina, C.C., Holt, J.R.*, et al.* (2011). Mechanotransduction in mouse inner ear hair cells requires transmembrane channel-like genes. J Clin Invest *121*, 4796-4809.

Kerstein, P.C., del Camino, D., Moran, M.M., and Stucky, C.L. (2009). Pharmacological blockade of TRPA1 inhibits mechanical firing in nociceptors. Mol Pain *5*, 19.

Kimitsuki, T., Nakagawa, T., Hisashi, K., Komune, S., and Komiyama, S. (1996). Gadolinium blocks mechano-electric transducer current in chick cochlear hair cells. Hear Res *101*, 75-80.

Kozlenkov, A., Lapatsina, L., Lewin, G.R., and Smith, E.S. (2014). Subunit-specific inhibition of acid sensing ion channels by stomatin-like protein 1. J Physiol *592*, 557-569.

Kurima, K., Peters, L.M., Yang, Y., Riazuddin, S., Ahmed, Z.M., Naz, S., Arnaud, D., Drury, S., Mo, J., Makishima, T.*, et al.* (2002). Dominant and recessive deafness caused by mutations of a novel gene, TMC1, required for cochlear hair-cell function. Nat Genet *30*, 277-284.

Lapatsina, L., Brand, J., Poole, K., Daumke, O., and Lewin, G.R. (2012). Stomatin-domain proteins. Eur J Cell Biol *91*, 240-245.

Liao, M., Cao, E., Julius, D., and Cheng, Y. (2013). Structure of the TRPV1 ion channel determined by electron cryo-microscopy. Nature *504*, 107-112.

Lu, Y., Ma, X., Sabharwal, R., Snitsarev, V., Morgan, D., Rahmouni, K., Drummond, H.A., Whiteis, C.A., Costa, V., Price, M.*, et al.* (2009). The ion channel ASIC2 is required for baroreceptor and autonomic control of the circulation. Neuron *64*, 885-

897.

Lucas, E.K., Reid, C.S., McMeekin, L.J., Dougherty, S.E., Floyd, C.L., and Cowell, R.M. (2014). Cerebellar transcriptional alterations with Purkinje cell dysfunction and loss in mice lacking PGC-1alpha. Front Cell Neurosci *8*, 441.

Maeda, N., Miyoshi, S., and Toh, H. (1983). First observation of a muscle spindle in fish. Nature *302*, 61-62.

Maingret, F., Patel, A.J., Lesage, F., Lazdunski, M., and Honore, E. (2000). Lysophospholipids open the two-pore domain mechano-gated K(+) channels TREK-1 and TRAAK. J Biol Chem *275*, 10128-10133.

McCarter, G.C., Reichling, D.B., and Levine, J.D. (1999a). Mechanical transduction by rat dorsal root ganglion neurons in vitro. Neurosci Lett *273*, 179-182.

McCarter, G.C., Reichling, D.B., and Levine, J.D. (1999b). Mechanical transduction by rat dorsal root ganglion neurons in vitro. Neurosci Lett *273*, 179-182.

Muller, K.A., Ryals, J.M., Feldman, E.L., and Wright, D.E. (2008). Abnormal muscle spindle innervation and large-fiber neuropathy in diabetic mice. Diabetes *57*, 1693-1701.

Oliveira Fernandes, M., and Tourtellotte, W.G. (2015). Egr3-dependent muscle spindle stretch receptor intrafusal muscle fiber differentiation and fusimotor innervation homeostasis. J Neurosci *35*, 5566-5578.

Owsianik, G., Talavera, K., Voets, T., and Nilius, B. (2006). Permeation and selectivity of TRP channels. Annu Rev Physiol *68*, 685-717.

Pan, B., Geleoc, G.S., Asai, Y., Horwitz, G.C., Kurima, K., Ishikawa, K., Kawashima, Y., Griffith, A.J., and Holt, J.R. (2013). TMC1 and TMC2 are components of the mechanotransduction channel in hair cells of the mammalian inner ear. Neuron *79*, 504-515.

Pepermans, E., and Petit, C. (2015). The tip-link molecular complex of the auditory mechano-electrical transduction machinery. Hear Res *330*, 10-17.

Poole, K., Herget, R., Lapatsina, L., Ngo, H.D., and Lewin, G.R. (2014). Tuning Piezo ion channels to detect molecular-scale movements relevant for fine touch. Nat Commun *5*, 3520.

Proske, U., and Gandevia, S.C. (2012). The proprioceptive senses: their roles in signaling body shape, body position and movement, and muscle force. Physiol Rev *92*, 1651-1697.

Proske, U., Wise, A.K., and Gregory, J.E. (2000). The role of muscle receptors in the detection of movements. Progress in neurobiology *60*, 85-96.

Rossi-Durand, C. (2006). Proprioception and myoclonus. Neurophysiol Clin *36*, 299-308.

Sakamoto, Y., Ishijima, M., Kaneko, H., Kurebayashi, N., Ichikawa, N., Futami, I.,

Kurosawa, H., and Arikawa-Hirasawa, E. (2010). Distinct mechanosensitive Ca2+ influx mechanisms in human primary synovial fibroblasts. J Orthop Res *28*, 859-864.

Siemens, J., Lillo, C., Dumont, R.A., Reynolds, A., Williams, D.S., Gillespie, P.G., and Muller, U. (2004). Cadherin 23 is a component of the tip link in hair-cell stereocilia. Nature *428*, 950-955.

Simon, A., Shenton, F., Hunter, I., Banks, R.W., and Bewick, G.S. (2010). Amiloride-sensitive channels are a major contributor to mechanotransduction in mammalian muscle spindles. J Physiol *588*, 171-185.

Sukharev, S., and Sachs, F. (2012). Molecular force transduction by ion channels: diversity and unifying principles. J Cell Sci *125*, 3075-3083.

Tourtellotte, W.G., and Milbrandt, J. (1998). Sensory ataxia and muscle spindle agenesis in mice lacking the transcription factor Egr3. Nat Genet *20*, 87-91.

Wetzel, C., Hu, J., Riethmacher, D., Benckendorff, A., Harder, L., Eilers, A., Moshourab, R., Kozlenkov, A., Labuz, D., Caspani, O.*, et al.* (2007). A stomatin-domain protein essential for touch sensation in the mouse. Nature *445*, 206-209.

Wilkinson, K.A., Kloefkorn, H.E., and Hochman, S. (2012). Characterization of muscle spindle afferents in the adult mouse using an in vitro muscle-nerve preparation. PLoS One *7*, e39140.

Woo, S.H., Lukacs, V., de Nooij, J.C., Zaytseva, D., Criddle, C.R., Francisco, A.,

Jessell, T.M., Wilkinson, K.A., and Patapoutian, A. (2015a). Piezo2 is the principal mechanotransduction channel for proprioception. Nat Neurosci *18*, 1756-1762.

Woo, S.H., Lukacs, V., de Nooij, J.C., Zaytseva, D., Criddle, C.R., Francisco, A., Jessell, T.M., Wilkinson, K.A., and Patapoutian, A. (2015b). Piezo2 is the principal mechanotransduction channel for proprioception. Nat Neurosci.

Woo, S.H., Ranade, S., Weyer, A.D., Dubin, A.E., Baba, Y., Qiu, Z., Petrus, M., Miyamoto, T., Reddy, K., Lumpkin, E.A.*, et al.* (2014). Piezo2 is required for Merkel-cell mechanotransduction. Nature *509*, 622-626.

Yang, Y.D., Cho, H., Koo, J.Y., Tak, M.H., Cho, Y., Shim, W.S., Park, S.P., Lee, J., Lee, B., Kim, B.M.*, et al.* (2008). TMEM16A confers receptor-activated calcium-dependent chloride conductance. Nature *455*, 1210-1215.

Yokoi, F., Dang, M.T., Yang, G., Li, J., Doroodchi, A., Zhou, T., and Li, Y. (2012). Abnormal nuclear envelope in the cerebellar Purkinje cells and impaired motor learning in DYT11 myoclonus-dystonia mouse models. Behav Brain Res *227*, 12-20.

Zimmerman, A., Bai, L., and Ginty, D.D. (2014). The gentle touch receptors of mammalian skin. Science *346*, 950-954.

국문초록

말초 신경계에서 기계적인 자극을 전기적 신호로 변환하여 인간의 뇌로 보내어 인지하는 데에는 기계적 자극의 수용기 (Mechanoreceptor)가 필수적이다. 이러한 Mechanoreceptor에는 모든 기계적 반응에 의하여 활성화되는 이온 채널 단백질 (Mechanosensitive ion channel, MS 이온 채널)이 존재하여 촉각, 청각 및 자가 수용 감각 등을 매개하며 그 분자 기전은 인간의 다양한 생리를 이해 하는데 필수적이다. 최근에 발견된 Piezo1과 Piezo2는 기계적 반응에 활성화되는 이온 채널 단백질로, 굉장히 빠르게 불활성화되며 인간의 촉감을 매개하는 것으로 알려졌다. 하지만 신경세포에는 아직 밝혀지지 않는 다양한 MS 이온 채널이 존재하고 있으며 오랜 기간 동안 이를 코딩하는 단백질을 찾아내지 못하고 있었다.

본 연구에서 생물 정보학적 방법을 이용하여 마우스 게놈에서 새로운 이온 채널 후보물질을 선별하였고, 후보 군에서 기계적 자극에 의해 활성화 되는 MS 이온 채널을 찾아내어 Tentonin 3 (TTN3) 유전자를 클로닝 하였다. TTN3는 이종 세포계에 과 발현 하였을 때 기계적 자극에 의해 활성화 되었고, 굉장히 느리게 불활성화되는 단백질임을 밝혀

내었다. TTN3 녹아웃 마우스를 제조하여 배근 신경절에 분포하는 신경세포에서의 표현형을 연구한 결과, Slowly Adapting Mechanosensitive 내향 전류 흐름이 큰 폭으로 감소하는 것을 확인하였다. 또한 TTN3에 의해 매개된 전류는 기존에 잘 알려진 MS 이온 채널 저해제에 의해 뚜렷하게 억제되었다. 마우스에서 표현형을 연구한 결과, 근육내의 근방추에서 TTN3의 발현을 확인하였고, TTN3 녹아웃 마우스의 움직임과 걸음걸이가 굉장히 둔화된 것을 알 수 있었다. 따라서 TTN3는 기계적 자극에 의해 활성화되고 굉장히 느리게 불활성화되는 유형의 MS 이온 채널이며 자가 수용 감각에서 그 역할을 하는 것으로 밝혀 내었다.

본 연구를 통하여 그동안 미지했던 분야인 기계적 수용 감각에 대한 실마리를 얻었고, 이를 통하여 인간의 운동 및 미세한 움직임의 매커니즘을 이해하는데 큰 역할을 할 것으로 사료된다.